Air quality simulation with WRF-Chem over southeastern Brazil, Part I: Model description and evaluation using ground-based and satellite data

[1] Noelia Rojas Benavente,

[2,3,4] Angel Liduvino Vara-Vela,

[5,6] Janaina P. Nascimento,

[7] Joel Rojas Auña,

[1] Aline Santos Damascena,

[1] Maria de Fatima Andrade and

[1] Marcia Akemi Yamasoe

[1] Departamento de Ciências Atmosféricas, Instituto de Astronomia, Geofísica e Ciências. Atmosféricas, Universidade de São Paulo, São Paulo, Brasil

[2] Department of Geoscience, Aarhus University, 8000 Aarhus, Denmark

[3] Department of Physics and Astronomy, Aarhus University, 8000 Aarhus, Denmark

[4] iCLIMATE Aarhus University Interdisciplinary Centre for Climate Change, Aarhus University, 4000 Roskilde, Denmark

[5] NOAA Global Systems Laboratory, Boulder, CO, USA

[6] Cooperative Institute for Research in Environmental Sciences, University of Colorado Boulder, Boulder, CO, USA

[7] Departamento de física interdisciplinaria, Universidad Nacional Mayor de San Marcos, Lima, Perú

Abstract

A comprehensive Weather Research and Forecasting with Chemistry (WRF-Chem) model evaluation is conducted using ground-based and total column observational data from air quality stations and satellite retrievals. Fine particles ($PM_{2.5}$; ≤ 2.5 μm in aerodynamic diameter), nitrogen oxides (NO_x, $NO + NO_2$), carbon monoxide (CO), tropospheric ozone (O_3) concentrations and AOD values over southeastern Brazil were analyzed to assess the model's capability in reproducing atmospheric observation. The model simulations were performed over simple one domain at grid resolution of 10 km over southeastern Brazil. This spatial resolution was chosen due to a previous evaluation between five MODIS AOD products with AERONET estimates, resulting in Dark Target at 10 km of spatial resolution the best product to represent the AOD values over our study domain. Model input emissions comprise vehicular emissions derived from a bottom-up emission model, as well as on-line calculations of biogenic and fire emission rates. Given that the atmospheric state affects air pollution dispersion,

a model evaluation on the meteorological conditions was carried out to better evaluate the model performance in reproducing the pollutant concentrations. Good agreement between model simulations and observations for air temperature and relative humidity at 2 meters height was found, with correlation coefficients higher than 0.85 in most periods. Expected benchmarks for wind speed and direction at 10 meters height were also found in this analysis, though with larger uncertainties. Underestimation occurred for daily accumulated precipitation due to the limitations of the cloud microphysics scheme or cumulus parameterization. Model simulations of $PM_{2.5}$, NO_x, CO and O_3 agreed well with ground-based observations in terms of temporal variations and trends, with model-observation discrepancies due to uncertainties in the emission inventories. O_3 was the better simulated pollutant in terms of temporal variability, with the characteristic large and small amplitudes observed over urban and rural areas being well represented by the model. High O_3 concentrations were observed at the Botucatu station, due to transport of pollutants generated in the Metropolitan Area of São Paulo, and were also represented by the model, indicating the need of more active air quality monitoring stations over inland regions in southeastern Brazil. Moderate and high correlation coefficients (ranging 0.46 - 0.81) were found for tropospheric NO_2 VCD and CO column, and AOD at 550 nm due to uncertainties in the emission inventories and aerosol model simplifications. Both the model and satellite captured higher values in similar regions over our study domain. This work represents a first effort, in southeastern Brazil, that combines numerical modeling, remote sensing and ground-based stations to analyze and understand the impact exerted by the emissions of urban pollution over surrounding areas. A more in-depth analysis of the impact of emissions transport to inland regions from urban areas in southeastern Brazil will be discussed in the second part of this work.

Keywords: Air pollution; WRF-Chem model; Air Quality station; AERONET; satellite products.

1. Introduction

Air pollution is a big problem, and although, in many places, the concentrations of pollutants are decreasing, they are still above the values recommended by the WHO (2021). This is basically related to population growth, mainly in urban and industrial areas where transportation and industries are often regarded as the main sources of air pollution (Lacasaña et al., 1999). The State of São Paulo, located in southeastern Brazil, has an area of approximately 249,000 km^2 (2.9 % of the national territory), a population of roughly 46.3 million inhabitants (22 % of Brazil) (IBGE, 2020), greater economic development (agricultural - especially sugar and alcohol, industrial and services) and the largest automotive fleet. Its air pollution can be attributed mainly to the vehicular fleet and industrial processes (Andrade et al., 2015). The Metropolitan Area of São Paulo (MASP), the largest urban center in Brazil, has a fleet of over 7 million vehicles (CETESB, 2019), representing one the major contributors to air pollution in this region (Pérez-Martínez et al., 2015). Past studies have shown that over the state of São Paulo, NO_x concentrations have reached a maximum value of 100 ppb, mainly rush hour traffic (Andrade et al., 2015; Vera-Vela et al., 2016; Gavidia-Calderón et al., 2018). NO_x is a primary pollutant and very difficult to evaluate due to the impact of local emissions from mobile sources on the concentrations measured at the air quality stations (Andrade et al., 2015; CETESB, 2021). This pollutant contributes to the O_3 formation, registering high concentrations of up 190 μg m^{-3} around 15 hours UTC. In the MASP, the anthropogenic fraction which emits VOCs is related to the use of fossil fuels by transportation and industrial processes (Brito et al., 2015 and Dominutti et al., 2020). Both the VOCs and NO_x act as O_3 precursors. On the other hand, $PM_{2.5}$ concentrations depend more on the formation of secondary aerosols (CETESB, 2021). High $PM_{2.5}$ concentrations can be registered by the air quality stations in São Paulo, produced by aerosol transport from biomass burns in the Amazon. Previous works have shown that the air quality in São Paulo has been affected by such events

(Nascimento, 2020; Vera-Vela et al., 2021). In relation to meteorological conditions, over the state of São Paulo, high pollutant concentrations are measured during the dry period, which is associated with favorable atmospheric conditions of less rainfall and high temperatures.

Since 1960, the MASP and other Brazilian cities began to grow more rapidly, generating a chaotic urbanization and an increase in sources of air pollution. To monitor the air quality in the State of São Paulo, an environmental agency (Companhia Ambiental do Estado de São Paulo, CETESB) was created in the late 1960s. Over a decade later, an air pollution control plan was designed to reduce the concentrations of particulates and sulfur dioxide (SO_2). The first action was the relocation of industrial plants located within urban centers to the interior of the State of São Paulo or to other Brazilian States. Cleaner technologies and production practices were then implemented in the industries to reduce their emissions and keep the related air pollutant concentrations within the primary air quality standards (CETESB, 2019). In 1975, the National Ethanol Program (PROALCOOL) was created in order to reduce CO emissions from the vehicle fleet, stimulating the use of ethanol as fuel (thus creating gasohol: a mixture of ethanol and gasoline) (Andrade et al., 2017). Later, in 1986, the National Council for the Environment (CONAMA) established the Programa de Controle de Poluição do Ar por Veículos Automotores (PROCONVE), a vehicle emission control strategy for the reduction of emissions from new vehicles, using air quality standards similar to the primary standards adopted by the US Environmental Protection Agency (https://www.epa.gov/criteria-air-pollutants/naaqs-table). Despite the efforts made to create several programs with the purpose of reducing both industrial and vehicular emissions, concentrations of secondary pollutants such as O_3 and $PM_{2.5}$ have not reduced over time (Andrade et al., 2012 ; Pérez-Martínez et al., 2015). Even though CETESB air quality monitoring network continuously operates throughout the State of São Paulo, the measurement sites are not spatially well distributed over the region. In this way, satellite remote-sensing technologies and chemical transport models represent powerful tools in monitoring air quality in rural or remote regions where no ground-based monitoring network exists (Chudnovsky et al., 2014). Although they provide limited quantitative information on air quality compared with ground-based monitoring (Valin et al., 2011; Benavente, 2014), they are useful for air quality research on identifying the location of peak concentrations and determining concentration gradients between surface monitoring stations (Benavente, 2014; Roy et al., 2017). Also, they can be used to evaluate the impacts of the regional transport of air pollutants from densely populated areas.

Several studies have applied the WRF-Chem model to simulate the air quality over MASP, most of them focusing on gaseous species (Silva et al., 2013; Albuquerque et al., 2018; Gavidia-Calderón et al., 2018; Schuch et al., 2018) and just a few on aerosols (Vara-Vela et al., 2016, 2018). Andreão et al. (2020) showed the relevance of using local anthropogenic emission inventories, where the distribution of pollutant plumes distinguishes local hot spots and spatial features that correlate with point sources and highways. Vara-Vela et al. (2016) evaluated the impact of vehicular emissions on the formation of $PM_{2.5}$ over MASP using the WRF-Chem model. They showed that the vehicular emission of primary gases led to the formation of secondary aerosol particles, with more than 40 % of the $PM_{2.5}$ formation being attributed to the emission of hydrocarbons (mainly aromatic). Gavidia-Calderón et al. (2018) evaluated the impact of using static and time-dependent chemical boundary conditions on WRF-Chem ozone simulations over MASP. They found that WRF-Chem performed better when time-dependent chemical boundary conditions were used, with improvements being more significant during periods with lower photochemical activity.

Regarding the use of remote sensing, there are several global observations available for a wide range of atmospheric pollutants (e.g., MODIS, MOPITT, OMI, among others). However, there are few studies (Damascena et al., 2021; Vara-Vela et al., 2018, 2021) that use satellite products together with model simulations

and ground-based stations to study air quality over southeastern Brazil, mainly over the MASP. This combination of tools will reinforce the understanding of the urban pollutants formation and transport, and how this urban pollution affects surrounding areas.

Therefore, the study focuses on assessing the model's capability in reproducing atmospheric pollutant concentrations and how they contribute to air pollution in nearby and far regions. We analyzed the spatial and temporal variability of NO_x, CO and O_3 and $PM_{2.5}$ concentrations and AOD values from ground-based stations and satellite retrievals. The model simulations were performed over a simple one domain at grid resolution of 9 km over southeastern Brazil during the dry season. Simulated data were compared against each other using a set of statistical indices and the study periods were chosen due to the availability of satellite data, shown in section 3.1. The results are presented in two papers. This first paper describes the model and the data sets used for the model evaluation. A second paper will focus on analyzing and understanding the transport from urban emissions to inland regions.

2. Methodology

2.1. Study area

The State of São Paulo has 21 % of the Brazilian inhabitants and is located in the southeast of Brazil. The MASP, one of the largest urban centers in the world, is located at around 23°S-latitude and 46°W-longitude within the State of São Paulo (Fig. 1). It has a total area of 7.946 km^2 (of which approximately 2.200 km^2 is highly urbanized) with an average altitude of 720 m (CETESB, 2017) above sea level. The city is on a plateau placed beyond the Serra do Mar, about 70 kilometers from the Atlantic Ocean. In some urbanized areas of São Paulo the terrain is roll, except in the northern area, where the Serra da Cantareira Range reaches a higher elevation. São Paulo is a disorganized urbanization and this caused an increase in the number of air pollution sources, which caused a critical situation in terms of air quality. The climate in the MASP is considered dry during the wintertime (between May and August), and wet during the summertime (between December and March). During the summertime, the precipitation over southeastern Brazil is often affected by the South American Monsoon System (SAMS) (Carvalho et al., 2011). During the wintertime, on the contrary high-pressure systems develop to the east, over the Atlantic Ocean, producing strong subsidence, thermal inversions and clear skies. As a consequence, few precipitation events (low relative humidity) are observed over the MASP during this time, thus favoring the formation of aerosol particles (CETESB, 2019).

2.2. The WRF-Chem model

The Weather Research Forecasting with Chemistry (WRF-Chem) (Grell et al., 2005) model is a fully coupled meteorology-chemistry transport model supported by the National Center for Atmospheric Research (NCAR) to a worldwide community of users. The Model for Ozone and Related Chemical Tracers (MOZART-4, (Emmons et al., 2010)) is selected for the gas-phase chemistry, coupled with the Goddard Chemistry Aerosol Radiation and Transport (GOCART, (Chin et al., 2002)) for aerosol chemistry. MOZART-4 mechanism includes 85 gas-phase species, 12 bulk aerosol compounds, 39 photolysis rates, 157 gas-phase reactions, in addition to an updated isoprene oxidation scheme and a better treatment of Volatile Organic Compounds (VOCs) (Emmons et al., 2010). Photolysis rates are calculated using the Fast Troposphere Ultraviolet Visible (F-TUV) photolysis scheme (Tie et al., 2003). GOCART is a bulk aerosol mechanism used to simulate the major tropospheric aerosol constituents such as: sulfur, dust, organic carbon (OC), black carbon (BC) and sea salt (Chin et al., 2002). No secondary organic aerosol (SOA) formation is treated in the GOCART model version used in this study.

2.2.1. Experiment design

The WRF-Chem model version 3.9.1 is used to perform 5-day simulations with initialization from previous runs on a single domain with a horizontal resolution of 9 km as shown in Fig. 1. The modeling domain is centered at 23.5°S and 46.3°W, is projected on a Lambert plane and consists of 150 grid points in the west-east direction, 100 grid points in the north-south direction, and 35 vertical levels that extend from the surface up to 50 hPa (20 km). Four different periods were selected according to the availability of observational data and favorable meteorological conditions for pollutant accumulation: a) from 00:00 UTC May 31 to 18:00 UTC June 30, 2017; b) from 00:00 UTC June 30 to 18:00 UTC July 31, 2018; c) from 00:00 UTC May 31 to 18:00 UTC June 30, 2019 and d) from 00:00 UTC July 31 to 18:00 UTC August 31, 2019. The first 24 hours in each run are discarded as spin-up time. The meteorological initial and boundary conditions to drive the simulations are obtained from the National Centers for Environmental Prediction (NCEP) Global Forecasting System (GFS) model at 0.25° horizontal resolution. For chemistry, the initial and boundary conditions are obtained from the Community Atmosphere Model with Chemistry model (CAM-Chem, (Lamarque et al., 2012)) at 0.9° x 1.5° horizontal resolution. These data have demonstrated the ability to represent tropospheric and stratospheric conditions including temperature structure and dynamics, using the MOZART-4 chemical mechanism (Emmons et al., 2010). Both NCEP GFS and CAM-Chem data are provided every 6 hours. The main physics and chemistry options used in this study are listed in Table 1.

2.2.2. Input emissions

As anthropogenic emissions over southeastern Brazil come mainly from ground transport (see Table S2 in the supplementary material), anthropogenic emissions from sectors other than ground transport (such as industrial and residential) are not included in the simulations. The ground transport emissions, specifically on-road vehicles, were derived from the bottom-up transport emission model described by Andrade et al. (2015). For more information, read section 2 in the supplementary material. Biogenic emissions are calculated on-line using the Model of Emissions of Gases and Aerosols from Nature (MEGAN) (Guenther et al., 2006). MEGAN estimates the net terrestrial biosphere emission rates for different trace gases and aerosols with a global coverage of 1 km^2 spatial resolution. Fire emission was derived from the Fire INventory from NCAR, hereafter referred to as FINN, as described by Wiedinmyer et al. (2011). This inventory provides fire emissions and plume rise characteristics of trace gases and aerosol particles from open biomass burning, including wildfires, agricultural fires, and prescribed burning, also on a global basis and resolution of 1 km^2 (Freitas et al., 2007; Grell et al., 2011). MEGAN and FINN emission maps for different gas and aerosol species are provided in the supplementary material, Figs. S18 to S21.

2.3. Observational Data

2.3.1. Ground-based observations

In the State of São Paulo, a network of air quality stations is responsible for the control and monitoring of the air quality, operated by the Companhia Ambiental do Estado de São Paulo (CETESB) (CETESB, 2019). CETESB manages 63 automatic air quality stations (61 fixed and 2 mobile) and 22 manual stations. The air quality stations (hereinafter referred to as AQS) provide hourly information on meteorological and pollutant parameters, such as air temperature at 2 meters (T_{2m}), relative humidity at 2 meters (RH_{2m}), wind speed and wind direction at 10 meters (WS_{10m} and WD_{10m}, respectively), and concentration of different air pollutants, such as nitrogen monoxide (NO), nitrogen dioxide (NO_2), tropospheric ozone (O_3), carbon monoxide (CO), fine particulate material ($PM_{2.5}$), among others (CETESB, 2019). These air quality and meteorological data are continuously published on the Qualar website (https://qualar.cetesb.sp.gov.br/qualar/home.do). In this work, 60 AQS spread

out across the State of São Paulo, mainly over the MASP (Fig. 1 and Table S1 - supplementary material), were selected for the analysis. Also, as addition stations (see Table 2), a meteorological station of the IAG-USP, located in the Parque de Ciência e Tecnologia from the University of São Paulo (in the south-east side of the MASP), and a mobile air quality station, located 200 km northwest of the MASP, on the outskirts of Botucatu, were considered in this work to analyze the WRF-Chem model performance. Both stations provide hourly data of meteorological parameters and chemical species (see Table 2). Moreover, to analyze aerosol columnar information, the Aerosol Robotic Network (AERONET) network was considered. AERONET program provides solar and sky radiance measurements in different wavelengths (340, 380, 440, 500, 675, 870 and 1020 nm) at 15-min sampling frequencies (Holben et al., 2001). To calculate the Aerosol Optical Depth (AOD) at 550 nm, solar direct measurements were used based on the Beer-Lambert-Bouguer law. For this work, we have considered four AERONET stations (see Table 2), a study period of six years (from 2014 to 2019) and data quality level 2.0 (cloud screened and quality-assured) to validate the WRF-Chem model simulations and the satellite aerosol retrievals.

2.3.2. Total column observations

Since atmospheric pollutants behave differently near the surface and far from it, the usefulness of satellite data to evaluate the WRF-Chem model is relevant. The Moderate Resolution Imaging Spectroradiometer (MODIS) sensor, the Ozone Monitoring Instrument (OMI) and the Measurements of Pollution In The Troposphere (MOPITT) were considered to compare the simulated values of AOD, NO_2 and CO, respectively. MODIS sensor measures the solar and terrestrial radiance, and through inversion algorithms, aerosol properties, including AOD are retrieved. These algorithms are: Dark Target (DT), Deep Blue (DB) and MAIAC. They estimate AOD values at 550 nm and at different spatial resolutions (1km, 3km, 10km and 1 degree) every 1-2 times per day. All of these products have level 2.0 data processing. For more details about these aerosol products, read the following articles (Kaufman et al., 1997, 2005a,b; Hsu et al., 2004, 2013; Lyapustin et al., 2018). On the other hand, OMI measures the radiation backscattered by the Earth's atmosphere and surface and uses different algorithms to retrieve atmospheric trace gases concentration, including NO_2, both in the troposphere and stratosphere, at 13km x 24km spatial resolution (Boersma et al., 2011). Here, we have considered retrievals of geolocated tropospheric VCD (vertical column density) NO_2 (in units of molecules cm^{-2}) extracted from the Dutch OMI NO_2 (DOMINIO v2.0) version 2.0 algorithm through the EUFP7 QA4ECV project. The DOMINIO data, Level 2 products, provide geophysical information for each and every ground pixel observed by the instrument. The product also contains intermediate results such as: a priori NO_2 profile, averaging kernel, among others, which will be explained in the next subsection. MOPITT measures the thermal infrared (IR) radiation with a spatial resolution of about 22km x 22km. These radiances are then used to retrieve CO mixing ratios profile and total column amounts (Deeter et al., 2003). For this work, we used version 9.0 Level 3 MOPITT CO mixing ratios at 10 pressure levels between the surface and 100 hPa, and with a spatial resolution of 1 degree. Another satellite product that will be compared to the WRF-Chem model outputs is the Global Precipitation Measurement (GPM) to analyze the daily accumulated precipitation over our study domain. The GPM mission provides global observations of rain and snow. The Integrated Multi-satellite Retrievals for GPM (IMERG) Final Run is an algorithm prepared to calibrate, mix and interpolate precipitation estimates from all passive-microwave instruments in the GPM Constellation (Huffman et al., 2015). IMERG covers the globe from 60°S to 60°N with a spatial resolution of 10km and a temporal resolution of 30 minutes and has three runs: early, late, and final. The early run (delay of 6 hours) employs morphing techniques that use the information from geostationary infrared data at a fine time scale to complete the gaps in coverage of microwave overpasses (Joyce et al., 2004). The late run (delay of 18 hours) allows additional microwave observations to be used in the morphing techniques. The final run (delay of 4 months), is adjusted to the monthly gauge measurements. In this study, we use version 6

GPM data to represent the final estimate of daily accumulated precipitation in mm (see Table 3). Almost all observational data have the same period as the WRF-Chem model simulations, except for aerosol products. AOD data was downloaded for a six-year period (2014 - 2019).

2.4. Data processing

The MODIS data validation has been made considering AOD data from AERONET stations, using the matching method. This type of method uses the closest pixel (granule of each satellite) to the location of an AERONET station and the AERONET data at an approximate satellite overpass time. Due to the lack of satellite and AERONET data and to increase the matchup data number, a spatiotemporal window has been adopted, following the approach devised by Ichoku et al., 2002. This methodology averages the satellite AOD data in a spatial window around the AERONET stations (1km, 3km and 10km) and the AERONET data is averaged in the temporal window centered on the satellite overpass time (±15, ±30 and ±60 minutes). The reason for choosing these spatial windows is because we use satellite data with a resolution of 1km up to 10km, so that all possible information can be considered (see Table 3). This comparison aims to show the best product to represent the aerosols over our domain and then compare it with the WRF-Chem simulations.

The WRF-Chem model was executed considering the pre-processing tools shown in Fig. S1 in the supplementary material. Overall, the modeling framework has three principal components: pre-processing, processing, and post-processing. The pre-processing defines the modeling domain, interpolates static geographical data and masked surface fields to the model grid, and prepares the meteorological, background concentrations, and emission fields to be read during the numerical integration. The processing is a program that must correctly incorporate the external fields prepared during the pre-processing, and then accurately simulate the state and chemical composition of the atmosphere. Finally, in the post-processing we read the model outputs using python scripts. To evaluate the performance of the WRF-Chem model when reproducing the pollutant concentrations and AOD values, we first evaluate the simulated meteorological variables with observational data (from CETESB, IAG-USP, Botucatu and GPM mission), taking into account that local meteorological variables strongly affect the transport and mixing of trace gases and aerosols (Banta et al., 2005; Darby, 2005). Then, simulated pollutant concentrations and AOD values were compared with ground-based (CETESB and Botucatu) and atmospheric column (MODIS, OMI and MOPITT) data. Due to the large number of AQS, both observed and simulated parameters were grouped and then averaged assuming four categories of land use: regional urban, urban park, urban and industrial (see Table S1 in the supplementary material). Air pollutants and meteorological parameters from the WRF-Chem simulations are extracted for the closest grid points to the AQS locations. To compare with atmospheric column data, mainly for NO_2 and CO, the model outputs must go through an appropriate treatment, since direct comparison between satellite retrievals with model data is not recommended (Kumar et al., 2012). This treatment comprises: (i) Due to the spatial resolution difference between the satellite and simulated data, it was necessary to perform a remapping of the gridded data. For NO_2, the satellite data were adjusted to the spatial resolution of the model, while for CO, the simulated data were adjusted to the spatial resolution of the MOPPIT. (ii) Since the model outputs and the satellite data have different temporal resolution, simulated data closer to passage time of each satellite have been considered to perform the comparison. (iii) Then, the model data were mapped onto the pressure grids of the different instruments (OMI and MOPPIT). (iv) Finally, the spatially and temporally matched model results were transformed using the averaging kernel (A) and a priori profiles used in the satellite retrievals to obtain a model profile. This last procedure was performed using the following equations:

$$Y_{trop} = A_{trop}.X_{trop}, \qquad where,\ A_{trop} = A.\frac{AMF}{AMF_{trop}} \tag{1}$$

$$X_{rtv-model} = X_a + A(X_{true-model} - X_a) \quad (2)$$

Equation (1) is applied for adjusting the WRF-Chem simulated tropospheric column NO_2 abundances for comparison to OMI retrievals, while the equation (2) is used to transform the WRF-Chem simulated column CO abundances for comparison with MOPPIT. A_{trop} is the total column averaging kernel, AMF and AMF_{trop} are the air mass factors for the total columns and tropospheric columns, respectively, Y_{trop} is the transformed model profile and X_{trop} is the tropospheric WRF-Chem NO_2 profile interpolated to the OMI pressure grid. All these variables are extracted from the satellite data of the DOMINIO v2.0 product. $X_{rtv\text{-}model}$ is the retrieved state vector and X_a and $X_{true\text{-}model}$ are the a priori state vector and the true state vector, respectively. **A** (in the equation 2) is the retrieval averaging kernel matrix and has a size of 10x10. It represents the sensitivity of the retrieved profiles to the actual profiles (Kumar et al., 2012; Ruibin et al., 2022; Tang et al., 2020). For comparison with the satellite AOD data, simulated and satellite data were remapped to the gridded data. The spatial resolution of the satellite data has been adjusted to have the same grid as the model (or vice versa) and the simulated data close to the passage of each satellite were selected. For comparison with AERONET AOD at 550nm, the simulated AOD at 550nm is derived from the WRF-Chem AOD at 300-, 400-, 600- and 1000-nm wavelengths, using the Angstrom equation (considering AOD at 400 and 600 nm). The same Angstrom equation was applied to AERONET AOD at 440 and 670 nm. In the case of precipitation data, both the model and the GPM provide data at the surface level. The simulated precipitation data was calculated by adding the "Accumulated total cumulus precipitation (RAINC)" and "Accumulated total grid scale precipitation (RAINNC)" outputs. These fields contain the total accumulated precipitation over the simulated period. Thus, the total accumulated precipitation is simply the sum of these fields (RAINC + RAINNC). Here, the model was also adjusted to the spatial resolution of the satellite by doing the remapping of the gridded data. In relation to the temporal resolution between the model and the satellite, the daily accumulated simulated precipitation was considered as the sum between 00:00 LT (Local Time) to 23:00 LT each day. These evaluations follow the performance benchmarks of Emery et al. (2017) and Monk et al. (2019), considering a simple and complex terrain (see Tables S3 and S4 in the supplementary material). The benchmarks for simple terrain were developed mostly for flat terrain and simple meteorological conditions. Instead, the benchmarks for complex terrain were developed for more complex conditions, considering mountainous terrain. The purpose of the benchmarks is to understand how good or bad our results are relative to other model applications run for the United States. We chose the most representative statistical indices (Appendix A) to compare them with these benchmarks.

3. Results and Discussions

3.1. Model performance for meteorological variables

Overall, the model adequately represented the temporal variability and trends of T_{2m} and RH_{2m} throughout the study periods as shown in Figs. 2 and 3, and S2 to S6 in the supplementary material. The WRF-Chem model qualitatively captured the strong changes in T_{2m} and RH_{2m} observed in all study periods, although it failed to properly represent the maximum and minimum peaks. Simulated surface temperature underestimated (Regional urban: MB = -0.20°C; urban: MB = -0.33°C; industrial: MB = -0.74°C) and overestimated (Regional urban: MB = 0.35°C; urban: MB = 0.11°C; industrial: MB = 0.23°C) the observed values for most of June 2017 and August 2019, respectively (see Table S5). However, in the urban park stations, the simulated surface temperature was overestimated in both June 2017 (MB = 0.08°C) and August 2019 (MB = 0.98°C). One of the reasons for this result could be the poor representation of land use considered by the model, which leads to higher temperatures than those measured by these AQS. In addition, the model and inventory resolution is an essential factor to recognize clearer emissions sources. The stations classified as urban park are Ibirapuera, Capão Redondo, Cid. Universitária-USP-Ipen and Itaquera (Table S1 in the supplementary material), all located near a green area

(between 158 – 300 km^2), while the model classified it as urban and built-up category (Fig. 1 - right panel). Similar differences in surface temperature and relative humidity were also verified in the Botucatu and IAG-USP stations (see Tables 5 and S6 in the supplementary material). The model overestimated and underestimated the observed surface temperature and relative humidity, respectively, in the IAG-USP station for all periods. The model, in Botucatu, showed the same behavior as the urban park stations, underestimating the observed surface temperature in June 2019 (MB = -1.17°C) and overestimating the observed surface temperature in August 2019 (MB = 0.47°C) (see Table 5). Regarding the wind speed and direction, Figs. 2 and 3, and S2 to S6 in the supplementary material, also show the comparisons between simulated and observed values. Both the simulated and observed wind speed had a strong diurnal variability, with higher values during the daytime and lower values during the nighttime. The simulated wind speed values ranged from 0.005 to 7 m s^{-1}, with a mean value of 3 m s^{-1}, indicating that winds were mostly weak during the study periods. The model overestimated (MB < 2 m s^{-1}) the wind speed, with shifts in wind direction fairly well reproduced most of the time. Overall, in terms of MB (see Figure S5 in the supplementary material), we can see that only for wind speed, the model overestimated the observed values for all of the region types and periods. For the other meteorological fields, the model underestimated and overestimated the observed values. The simulated meteorological fields can be biased, with errors in characteristic varieties in seasonal and diurnal verification depending on the WRF model configuration and meteorological conditions. The over-predicting surface wind often results from imperfect land surface processes and resolving topography. This underestimation and/or overestimation are consistent with the large negative and/or positive bias in previous investigations (Martins L. D. et al., 2006, 2018; Vara-Vela et al., 2016, 2018, 2021; Gavidia-Calderón et al., 2018, 2021). Worst and best model performance took place at urban park (including the IAG-USP station) and regional urban (including Botucatu station), respectively (see Figure S5 and Tables 5 and S6 in the supplementary material).

Considering the benchmarks recommended by Monk et al. (2019) (Table S3 in the supplementary material), the WRF-Chem model fulfilled the expected benchmarks, mainly for the temperature, relative humidity and wind speed (shown in the Table 5 and Tables S5 and S6 in the supplementary material). For the wind direction, the model did not fulfill the expected benchmarks, mainly over industrial areas. The model's performance evaluation for accumulated precipitation (Figs. 4 and 5) shows that the model was able to reproduce days with rain events on local and regional scale, although large differences in accumulated precipitation between observations and model simulations were observed. Clouds representation in models remains a challenging task, current models are not capable of quantitatively representing precipitation events (Tie et al., 2009; Freitas et al., 2021). Model-observation discrepancies are strongly associated with the misrepresentation of land use and stability (Molders et al., 2010), as well as with differences in geographical locations between model grid-points and AQS.

3.2. Model performance for pollutants and AOD retrievals

3.2.1. Comparison with ground-based measurements

As shown in Figs. 6 and 7, and S7 and S8 in the supplementary material, the temporal variations and trends in NO_x and O_3 concentrations were well represented by the model. With the exception of O_3, all the other pollutants had their observational concentrations significantly higher in urban areas than in rural areas, and this behavior was well reproduced in the simulations. For most periods (see Table 6), simulated NO_x concentrations were underestimated in regional urban, urban and industrial areas, and were overestimated in urban parks. For model-based assessments of both urban and rural NO_x concentrations, it is important to be able to simulate daily maximum urban and NO_x rural background concentrations as well. In order to assess the model's skill in reproducing these concentrations, we compare simulated diurnal cycles of NO_x (Fig. S10 in supplementary material). The comparisons showed that the model was able to simulate the observed diurnal cycle in the

regional urban, urban and industrial areas, while it did not have a good performance at urban park area. The model overall overestimated the NO_x concentrations in the urban park and urban areas around 7:00 and 19:00 LT (in the peak hours) and underestimated the observed values at urban areas during afternoon. Due to the low horizontal resolution, the model calculated unrealistic peaks of NO_x concentrations in traffic hours at urban park areas. The contribution to the overestimating and underestimating during daytime might be related by various factors, such as emissions inventories, uncertainties in the meteorological fields and the model's limitations. Both the model and the emissions inventory resolutions play a key role in simulating urban and rural NO_x concentrations during daytime. As more NO_x is emitted at the streets, rather than at the edges of the city, the correct concentration can hardly be calculated with emission input data of a horizontal resolution of 9 km. Furthermore, the temporal profile used to distribute the emissions over the modeling domain is the same in all grid points with any emission value (see Figs S16 and S17 in the Section 2 in the material supplementary).

Figure 8 shows a spatial distribution of surface NO_x and O_3 from CETESB stations and WRF-Chem simulations at 18:00 LT, which corresponds to the second rush hour (see Figure S10 in the supplementary material) .We can observe a good representation between both data during the four study periods. High concentrations of observed and simulated NOx were captured within MASP (urban areas), while low concentrations were observed outside the MASP (regional areas). These analyzes indicate that the use of the vehicle emissions inventory (see section 2 in the supplementary material) was fairly well estimated on the MASP. The model was able to represent the O3 spatial distribution, with both observations and simulations ranging from 90 to 120 μg m^{-3}. The simulated O_3 concentrations showed the best results in terms of correlation coefficient ($R \geq 0.79$), reaching the goal performance benchmark suggested by Emery et al. (2017) (Table S4 in the supplementary material). This is consistent with previous studies, showing the good performance of the model when calculating O_3 concentrations over the State of São Paulo (e.g. Vara-Vela et al., 2016; Gavidia-Calderón et al., 2018). However, they also found small differences between the model and the observations, similar to this work. Here, O_3 concentration was overestimated throughout the study periods ($\overline{MB}$= 22 μg m^{-3}), mainly over regional urban and industrial areas. These discrepancies are basically due to the choice of the appropriate chemical mechanism. The bias between observed and simulated O_3 concentration is consistent with the bias in NO_x diurnal cycle concentration discussed above. The underestimation of O_3 during the night in urban park and urban areas is consistent with an overestimation of NO_x. However, the overestimation of O_3 in the morning hours could be due to too much NO_2 accumulated on the surface, which is photolyzed when the sun rises. Therefore, the model successfully reproduced the O_3 diurnal pattern, indicating strong O_3 build-up from sunrise to noontime (peak of 90 μg m^{-3}) and the predominance of titration chemistry and deposition losses at night. The model also reproduced the daily amplitude of O_3 concentration changes at relatively cleaner stations such as Botucatu, where it is typically shown a less pronounced O_3 diurnal variability due to reduced NO_x emissions. The simulated O_3 concentrations agreed well with the high concentrations observed at Botucatu during August 2019 (Fig. 7). Part of these high O_3 concentrations was caused by the regional transport from the MASP (Squizzato et al., 2021). A more detailed analysis will be discussed in the second part of this article. This result showed the importance of using comprehensive modeling tools to evaluate the impact of regional emission transport from large urban areas.

Regarding simulated and observed CO and $PM_{2.5}$ concentrations, they were significantly higher in urban than in rural areas, although the model underestimated the observed values for both pollutants in all stations. The underestimation of CO is directly related to the emissions inventory over our study area, while the bias of simulated and observed $PM_{2.5}$ concentrations is related to the choice of aerosol mechanism used in the simulations (Tie et al., 2013; Mar et al., 2016; Vara-Vela et al., 2018). On the other hand, the model

underestimated the hourly concentrations of these pollutants most of the time ($\overline{MB}$ of -0.28 ppmv for CO and -8.18 μg m^{-3} for $PM_{2.5}$). It is important to mention that the model was able to represent the rapid increase in the concentrations during strong air pollution events (urban park and urban areas in Fig. 6). In relation to the diurnal cycle of CO and $PM_{2.5}$ between the observed and simulated values, Fig. S11 in the supplementary material, shows that the model represented well the observed CO variability, calculating peaks of CO in traffic hours, mainly at urban areas. In terms of correlation coefficient, the daily $PM_{2.5}$ concentrations reached the criteria ($R \geq 0.40$) and goal ($R \geq 0.70$) performance benchmark suggested by Emery et al. (2017), with June 2017 showing the best result among all study periods (see Table 4). These results represent a great contribution to previous modeling studies (Martins et al., 2006, 2018; Vara-Vela et al., 2016, 2018, 2021; Gavidia-Calderón et al., 2018, 2020) demonstrating that the model can satisfactorily represent the atmospheric dynamic, chemistry and boundary layer processes.

3.2.2.Comparison with atmospheric column measurements

Figs. 9 to 11, and S12 to S13 in the supplementary material show the simulated and observed column mass abundances of NO_2 and CO, and AOD values over southeastern Brazil for the four study periods. The spatial discrepancies between simulated and observed fields are illustrated by the relative differences shown in the third column of these Figures. Both the model and satellite retrievals showed higher tropospheric NO_2 VCD in regions of industrial activities and/or dense population (10×10^{15} molecules cm^{-2}), within the MASP. Also, they showed lower values over the center of the State of São Paulo and less urbanized regions (by about 2×10^{15} molecules cm^{-2}) (see first and second columns in Fig. 9). The model also captured the monthly decrease, similar to the OMI, from the first to the fourth study period. The spatial correlation averaged over the entire domain ranged between 0.64 (in June and August 2019) and 0.77 (July 2018), obtaining from moderate to high correlation coefficients (see also in Table 6). In terms of bias, it was demonstrated that the WRF-Chem underestimated the magnitude of the retrieved tropospheric NO_2 VCD over most of the study domain for all study periods. Highest NMB (-68.09 %) and NME (68.92 %) values were found for August 2019. These large model-satellite differences were associated with the poor representation of the contribution of long-range transport of biomass burning from the Amazon which affected the air quality over the State of São Paulo, mainly during 19 and 20 August 2019, as described in (Vara-Vela et al., 2021). Other sources of difference can arise from errors in simulating tropospheric NO_x chemistry (Valin et al., 2011) and other anthropogenic emission sources such as soil NO_x.

The spatial distributions of simulated and MOPITT-retrieved CO VCD (integrated up to 100 hPa) are shown in Figs. 10 and S12. Both the model and satellite show a homogeneous spatial distribution with values of CO from 1.1 up to 1.7×10^{18} molecules cm^{-2} during the afternoon (around at 14:00 LT - Fig.10) and evening (around at 22:00 LT - Fig. S12) periods. The model slightly overestimated the satellite estimates for all study periods, with averaged MB of 0.14×10^{18} molecules cm^{-2}. A good spatial correlation between the model and satellite estimates were found, with an average correlation coefficient of 0.71 and a NMB < 10 %. The agreement between WRF-Chem and MOPITT is higher in July 2018 (NMB = 8.17 %) than June 2017 (NMB = 14.05 %). For August 2019, MOPITT CO data was not available.

Regarding AOD, simulated values were compared against MODIS and AERONET retrievals. Looking at the comparison between WRF-Chem and MODIS AOD values (Figs. 11 and S13 in the supplementary material), both the model and MODIS sensor show low AOD values during all study periods. In addition, the model was not able to produce high AOD episodes (see Fig. 11). SOA formation is not treated in the aerosol module, and represents, together with an underestimation in the emissions inventory, the major sources of uncertainty in the

aerosol modeling. Domain-wide correlation ranged between 0.44 (Terra satellite) and 0.65 (Aqua satellite) in August 2019, and 0.70 (Terra satellite) and 0.75 (Aqua satellite) in July 2018 (see Table 7). As discussed above, the model did not represent the contribution of long-range transport of biomass burning in August 2019. This reflects the low correlation between the model and MODIS. The simulated AOD values were lower than MODIS estimates, with an averaged NMB of -39.15 % and -24.25 %, for Terra MODIS and Aqua MODIS, respectively.

On the other hand, due to the limited AERONET data availability, we compared the AOD values of both models, MODIS sensor and AERONET network (Fig. S14). Fig. S14 in the supplementary material shows boxplots of the WRF-Chem, Terra-Aqua and AERONET AOD values for June 2017 over the AERONET stations. We can observe that the average values for all of the points registered at São Paulo, SP-EACH and Itajuba stations, estimated via the WRF-Chem model, were in general underestimated. For the Terra satellite, i.e. during morning overpasses, the AOD values at São Paulo and SP-EACH stations presented lower variability than AERONET retrievals, while the opposite was observed during Aqua overpasses. Among the gas and aerosol analyzed parameters, the $PM_{2.5}$ and AOD are the most difficult to simulate, as aerosol life processing depends on multiple atmospheric processes such as secondary organic aerosol (SOA) formation (Kanakidou et al., 2005). Knowledge gaps in aerosol modeling in terms of formation and aging processes, including aerosol feedback effects on meteorology and radiation, represent other sources of uncertainty (Vara-Vela et al., 2021). As the temporal profile used to distribute the emissions over the modeling domain is the same, this limitation can lead to possible mismatches between model predictions and satellite observations in regard to the timing of peak of AOD values at any particular time and location.

Besides emissions and meteorology, the choice of the chemical mechanisms plays an important role in the simulation of air pollutants. For example, Vara-Vela et al. (2016) and Gavidia-Calderón et al. (2018) using the WRF-Chem chemical mechanisms Regional Acid Deposition Model version 2 (RADM2; (Chang et al., 1990)) and Carbon-Bond Mechanism version Z (CBM-Z; (Zaveri et al., 1999)), respectively, and emission approaches similar to that used in this study, have found that the model underestimated and overestimated, respectively, the O_3 concentrations at several AQS across the MASP. In general, an underestimation of NO_x and CO was related to a lack of emission sources, while an overestimation in the concentration of these pollutants could be related to either inaccurate representations of emissions or meteorology, or a combination of both (Kota et al., 2014; Changhan et al., 2020; Nascimento et al., 2020). In addition to inaccurate representations of emissions and meteorology, model bias in simulating O_3 and $PM_{2.5}$ depends on the photochemistry, VOCs speciation assumptions used in the chemical mechanisms and also the atmospheric dynamics and photochemistry to determine the gross production of those secondary pollutants (Nascimento et al., 2022). Most chemical mechanisms make use of lumping approaches to reduce the number of chemical reactions, thus avoiding the treatment of a huge number of chemical species (Zaveri et al., 1999; Sarkar et al., 2016). On the other hand, the use of a more simplified gas-phase chemistry, photolysis and dry deposition schemes in chemical transport models does not guarantee an improvement in the model predictions (Vara-Vela et al., 2016, 2018; Gavidia-Calderón et al., 2018).

4. Conclusions

A six-year study (2014-2019) period has been selected to validate five MODIS AOD products against AERONET estimates over southeastern Brazil, with focus on the Metropolitan Area of São Paulo. Considering the greater availability of MODIS data and using a matching methodology, we have shown the best MODIS product to represent AOD values over southeast Brazil, mainly for dry periods (section 3 in the supplementary material). Results showed that the Dark Target product at 3 km and 10 km spatial resolution better represented

the AERONET AOD estimates compared to the other products. WRF-Chem AOD simulations were compared to the Dark Target product with 10 km x 10 km spatial resolution to minimize the numerical instabilities. One-month WRF-Chem simulations at 9 km for June 2017, July 2018, and June and August 2019, were then evaluated against the Dark Target product at 10 km and observational data from ground-based platforms over southeastern Brazil. In relation to ground-based measurements, the strong changes in temperature and relative humidity at 2 m observed in the four study periods were satisfactorily represented by the model, although it failed in representing the maximum and minimum peaks. The model underestimated the temperature over regional urban, urban and industrial areas, while it overestimated the temperature over urban park areas for most of the periods, with the exception of August 2019. The model overestimated the temperature with an average bias of less than 1°C for all periods, a result that is in line with previous WRF-Chem studies over southeast Brazil. Simulated wind speed and direction at 10 m were well represented by the model in terms of spatial and temporal variation and trends. Both observed and simulated wind speed were more intense during the daytime and relatively calm during nighttime. Model-observation discrepancies are strongly associated with the misrepresentation of land use and stability, as well as with differences in geographical locations between model grid-points and air quality stations. However, our modeling results fulfilled the expected benchmarks performance.

Regarding air pollutants, the model was able to represent the temporal variations and trends of most of the chemical species, including CO, O_3, $PM_{2.5}$ and NO_x. However, model-observation discrepancies were also noticeable, with NO_x underestimation over regional urban and urban stations, and overestimation over industrial stations. The O_3 was the best air pollutant to be simulated in terms of temporal variability, with large and small amplitudes observed over the MASP (as urban area) and Botucatu (as rural area) being well represented by the model. The model satisfactorily represented the high O_3 concentrations observed at Botucatu station, indicating the importance of using comprehensive modeling tools to evaluate the impact of large urban centers emissions in the regional transport of pollutants. The CO concentrations were significantly underestimated most of the time. Overall, an underestimation of NO_x and CO is related to a lack of emission sources, while an overestimation in the concentration of these pollutants could be related to either inaccurate representations of emissions or meteorology, or a combination of both. Similar to CO pollutants, the simulated $PM_{2.5}$ concentrations were also underestimated most of the time. In addition to inaccurate representations of emissions and meteorology, model bias in simulation of O_3 and $PM_{2.5}$ depends on the photo-chemistry and VOCs speciation assumptions in the chemical mechanisms.

The comparison between atmospheric column observations of NO_2 and CO from OMI and MOPPIT instruments, respectively, and WRF-Chem during the four study periods showed that the model agreed well with satellite estimates, even though the model underestimated or overestimated the retrieved concentrations in some cases. Both the model and OMI captured higher NO_2 VCD concentrations in regions with industrial activities and/or dense population and lower NO_2 VCD concentrations over less urbanized areas. Regarding CO column data, both the model and the satellite showed a homogeneous spatial distribution during all study periods, resulting in high correlation coefficient (mean: $R = 0.71$). For AOD, both WRF-Chem and MODIS (Terra and Aqua) detected higher AOD values over the ocean and lower AOD values over the continent. However, on days with high MODIS AOD values over the continent, the model was not able to represent them properly. The inclusion of sea salt emissions in the model simulations contributed to a better representation of aerosol loadings over the ocean, while, over the continent, an underestimation of AOD is to a large extent due to no inclusion of SOA formation. The spatial correlation coefficients ranged from 0.44 and 0.75. The WRF-Chem model showed deficiency in representing aerosols at the four specific AERONET stations, with lower correlation coefficients compared to those found for satellite estimates. Discrepancies between model and observations at site-specific

locations at both surface and total-column can be also related to a misrepresentation of local conditions, not only in terms of emissions but also in terms of land-use and atmospheric stability. Overall and in spite of model-observation discrepancies, we can conclude that the WRF-Chem model was able to detect high aerosol concentration events at regional scale. Model underestimations are in general related to an underestimation in the emissions calculation, highlighting the need for more accurate aerosol emissions representation over a metropolitan area with complex and distinct anthropogenic contributions. Based on the findings of this study, the use of up-to-date and high spatiotemporal resolution anthropogenic emission inventories is recommended for forecasting the concentrations and the diurnal fluctuations of atmospheric pollutants, especially near the urban centers where the majority of population lives.

This work represents a first effort combining different tools: ground-based observations, numerical modeling and remote sensing, to improve the understanding of how pollutant emissions impact the air quality over the Metropolitan Area of São Paulo and inland areas (which will be discussed in detail in the second part of this work). Consequently, future efforts for a regional and/or local study should consider local emission inventories as they provide better results compared to regional inventories. In addition, monitoring air quality in less urbanized areas must be an ongoing effort to validate numerical modeling of long-range transport of emissions from large urban areas such as the Metropolitan area of São Paulo.

5. Declaration of Competing Interest

The authors declare that they have no known competing financial interests or personal relationships that could have appeared to influence the work reported in this paper.

6. Acknowledgements

We greatly appreciate the financial support provided by FAPESP (process number 2016/18438-0) and the Coordination for the Improvement of Higher Education Personnel (CAPES) Program. Thanks also to the staff of the AERONET network for the free aerosol data, to the CETESB team, especially the pioneers, who throughout these years had contributed for freely spreading the monitoring of air quality over the State of São Paulo. Finally, thanks to the team of the WRF-Chem model for the constant updating of the versions of the photochemical model and for the facilities they offer us to handle it. MAY acknowledges the National Council for Scientific and Technological Development (CNPq) fellowship process numbers 313005/2018-4 and 311984/2021-5.

Appendix A – Performance metrics

The focus of the model evaluation is mainly to verify the capacity of the model to effectively reproduce the spatial and temporal distribution of pollutant concentrations observed over the State of São Paulo, in particular over the MASP. Therefore, statistical evaluation metrics such as the Pearson correlation coefficient (R), root mean square error (RMSE), mean bias (MB), normalized MB (NMB), average MB ($\underline{MB}$), mean error (ME), normalized ME and index of agreement (IOA), were used to evaluate the WRF-Chem model performance on a regional scale. These statistical indicators were calculated using the following equations (Emery et al., 2017):

$$R = \frac{\sum_{i=1}^{N}(pred_i - \overline{pred}_i)(obs_i - \overline{obs}_i)}{\sqrt{\sum_{i=1}^{N}(pred_i - \overline{pred}_i)^2 (obs_i - \overline{obs}_i)^2}}, \qquad \text{Unitless } -1 \le R \le +1 \quad (A.1)$$

$$RMSE = \sqrt{\frac{\sum_{i=1}^{N}(pred_i - \overline{pred}_i)^2}{N}}, \qquad 0 \le RMSE \le \infty \quad (A.2)$$

$$MB = \frac{\sum_{i=1}^{N}(pred_i - obs_i)}{N}, \qquad -\infty \le MB \le \infty \quad (A.3)$$

$$NMB = \sum_{i=1}^{N}\frac{(pred_i - obs_i)}{obs_i} x100, \qquad -100\ \% \le NMB \le +\infty \quad (A.4)$$

$$ME = \frac{\sum_{i=1}^{N}|pred_i - obs_i|}{N}, \qquad 0 \le ME \le \infty \quad (A.5)$$

$$NME = \sum_{i=1}^{N}\frac{|pred_i - obs_i|}{obs_i} x100, \qquad 0\% \le NME \le \infty \quad (A.6)$$

$$IOA = 1 - \frac{\sum_{i=1}^{N}(pred_i - obs_i)^2}{\sum_{i=1}^{N}(|pred_i - \overline{pred}_i| + |obs_i - \overline{obs}_i|)^2}, \qquad \text{Unitless } 0 \le IOA \le +1 \quad (A.7)$$

The $pred_i$ and obs_i are the simulated and observed data, respectively. The $\overline{pred}_i$ and $\overline{obs}_i$ are the corresponding mean values. "N" is the number of paired samples. R = 1 is a perfect correlation; R = 0 is totally uncorrelated.

Figures

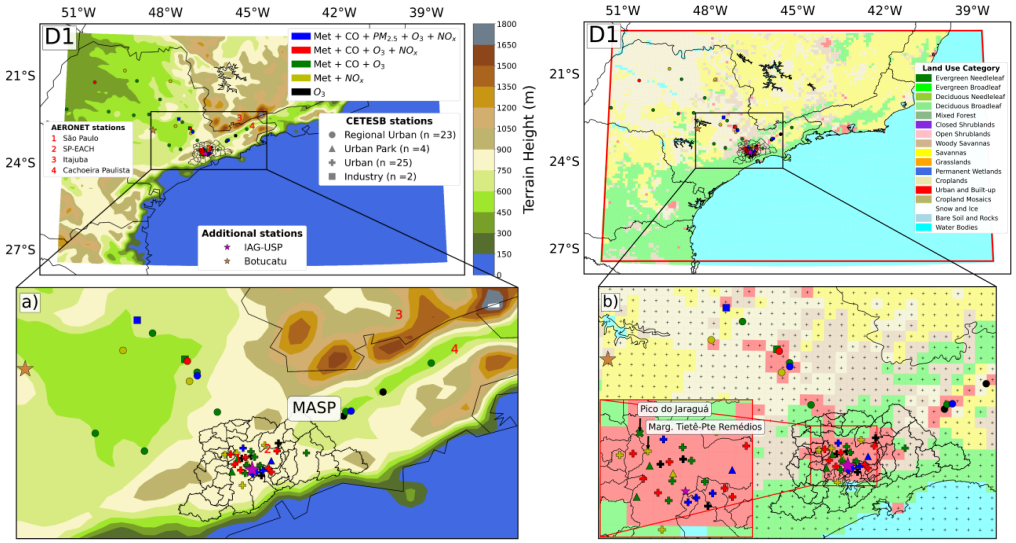

Figure 1: (a) The terrain height and (b) land use category map of the model domain (D1) considered in the WRF-Chem model and the locations of the CETESB and AERONET monitoring stations.

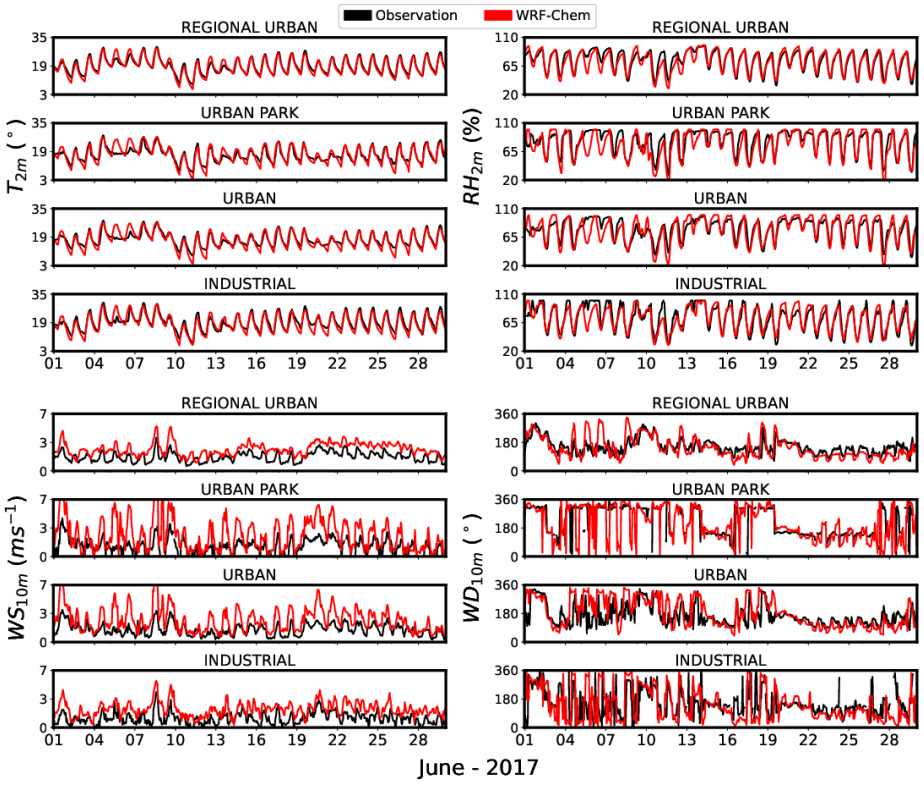

Figure 2: The observed and simulated T_{2m}, RH_{2m}, WS_{10m} and WD_{10m} variability in the four categories of land use: Regional urban, urban park, urban and industrial, during June 2017. The measured and simulated results are represented by the black and red line, respectively.

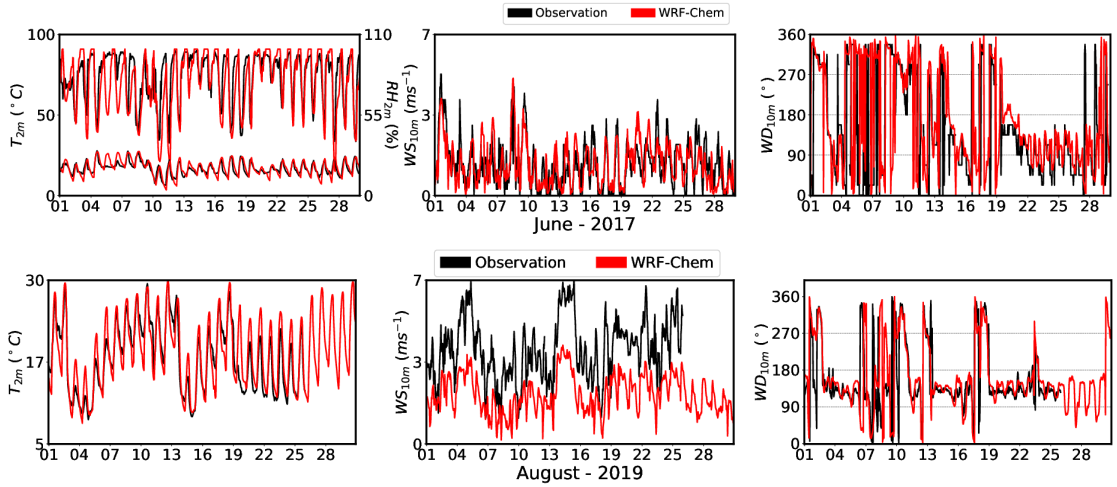

Figure 3: The observed and simulated meteorological variability at the IAG-USP and Botucatu stations during June 2017 and August 2019, respectively. The bars represent the daily accumulated precipitation. The measured and simulated results are represented by the black and red line, respectively.

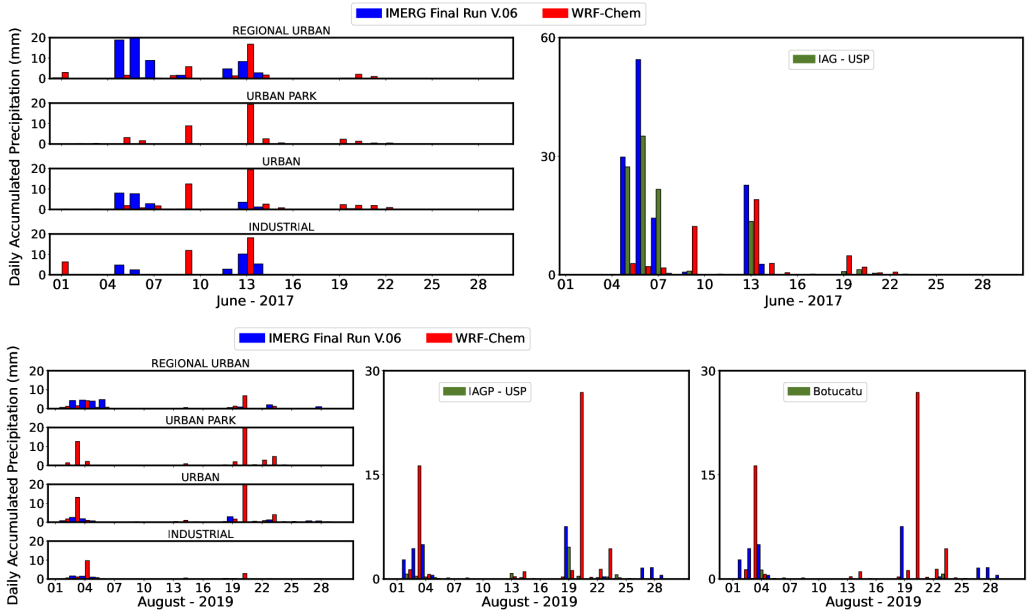

Figure 4: The observed and simulated daily accumulated precipitation (mm) variability at the IAG-USP and Botucatu stations during June 2017 and August 2019, respectively. The bars represent the daily accumulated precipitation. The measured and simulated results are represented by the black and red line, respectively.

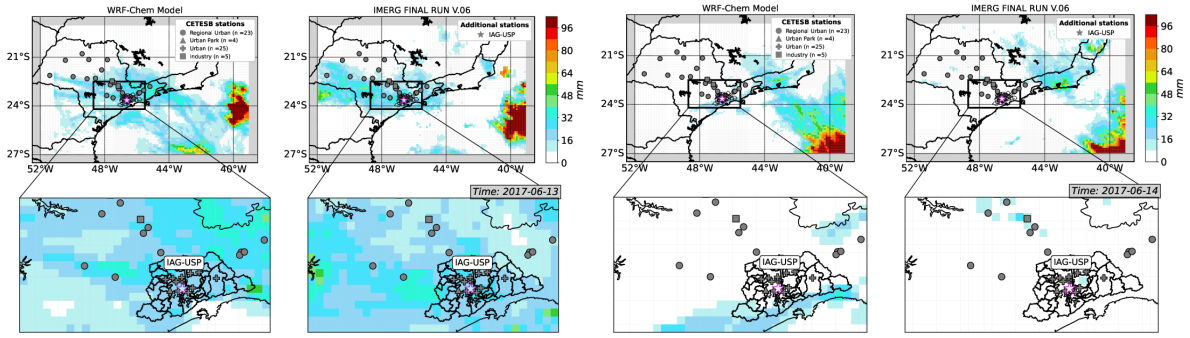

Figure 5: Spatial distribution of daily accumulated precipitation (mm) from WRF-Chem model and IMERG Final Run V.06 product over southeastern Brazil for 13 and 14 June, 2017. The black square represents the zoom of the MASP. The gray dots represent the AQS distributed over our study area and the magenta star represents the location of the IAG-USP station.

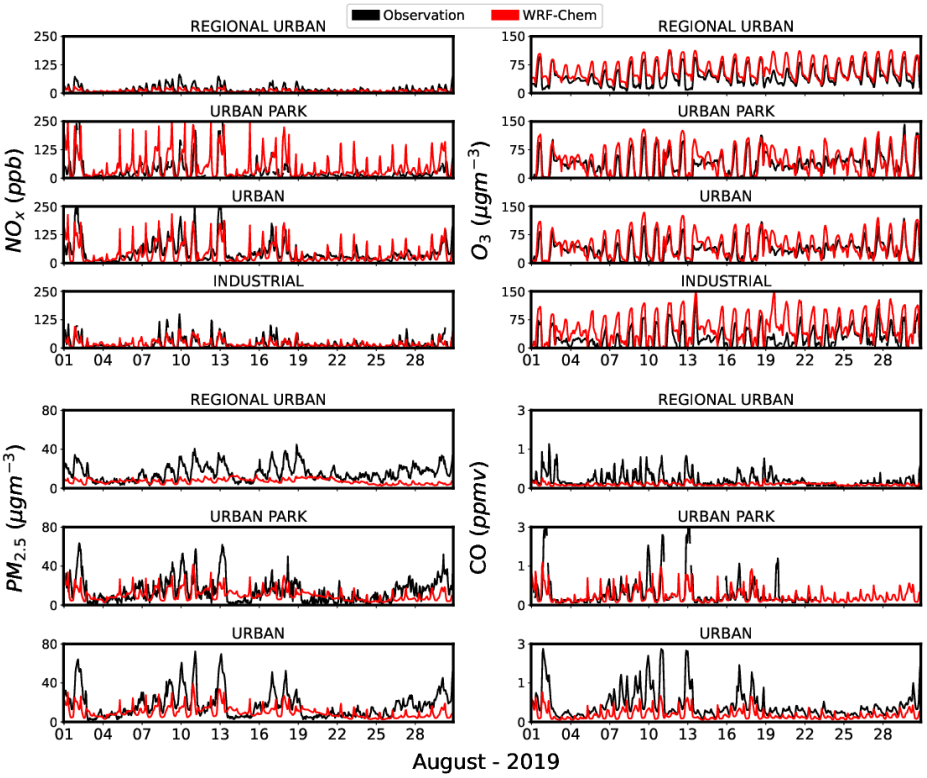

Figure 6: The observed and simulated NO_x, O_3, $PM_{2.5}$ and CO concentrations variability in the four categories of land use: Regional urban, urban park, urban and industrial, during August 2019. The measured and simulated results are represented by the black and red line, respectively.

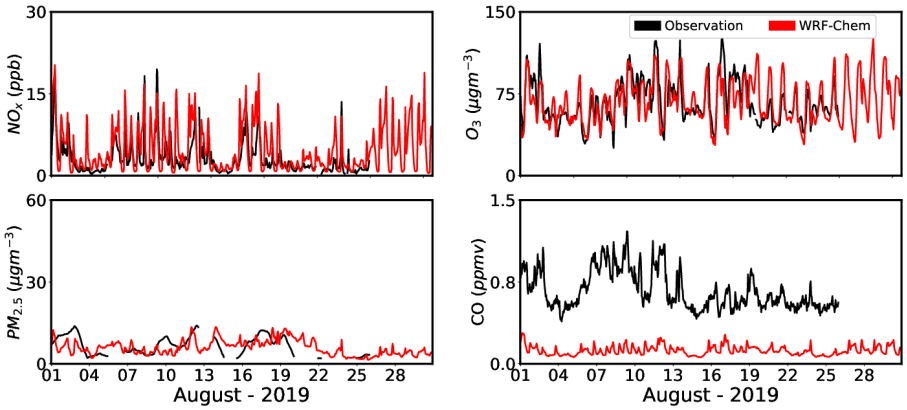

Figure 7: The observed and simulated NO_x, O_3, $PM_{2.5}$ and CO concentrations variability at Botucatu station during August 2019. The measured and simulated results are represented by the black and red line, respectively.

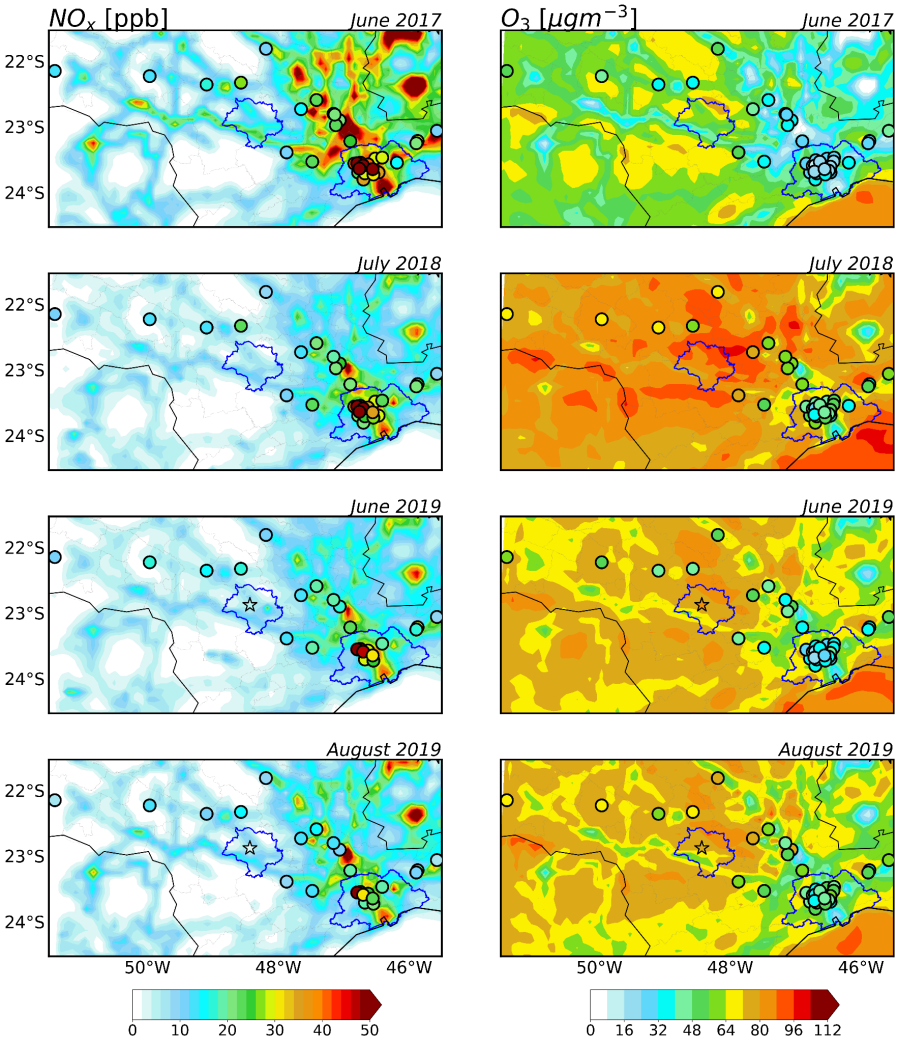

Figure 8: Simulated and observed (colored circles) monthly spatial distribution of surface NO_x (first column) and O_3 (second column) at 18:00 LT, which corresponds to the second rush hour over southeastern Brazil for June 2017, July 2018 and June and August 2019. The colored circles represent the CETESB stations distributed in the state of São Paulo and colored stars represent the Botucatu station. The blue outlines, in the columns, represent Botucatu city and the MASP.

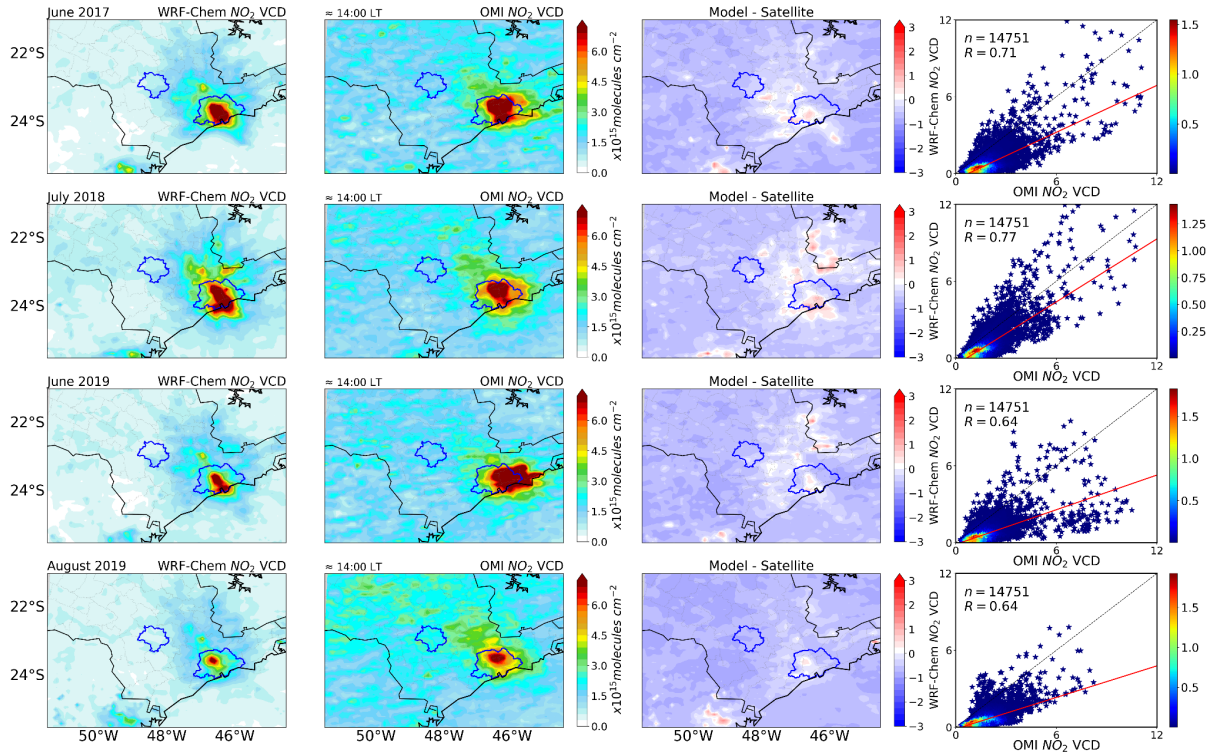

Figure 9: Simulated (first column) and observed (second column) mean spatial distribution of tropospheric NO_2 VCD during 14:00 LT over southeastern Brazil for June 2017, July 2018 and June and August 2019. The third and fourth columns represent the relative difference and correlation between both tools. The blue lines, in the first three columns, represent Botucatu city and the MASP and the gray space indicates missing data.

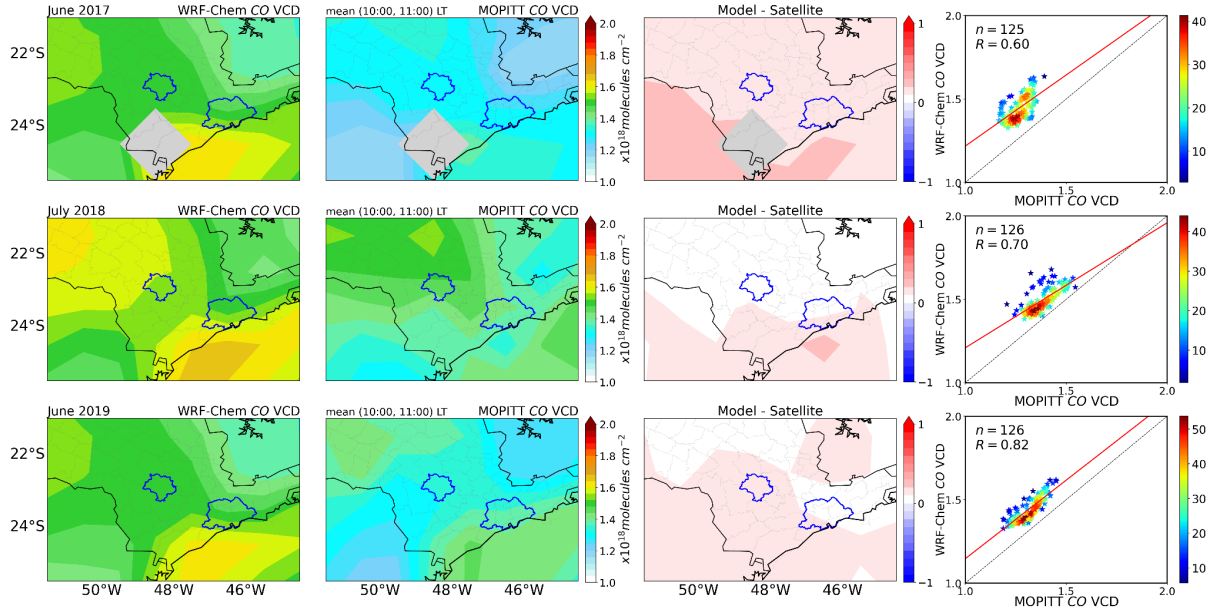

Figure 10: Simulated (first column) and observed (second column) mean spatial distribution of total CO VCD during 14:00 LT over southeastern Brazil for June 2017, July 2018 and June 2019. The third and fourth columns represent the relative difference and correlation between both tools. The blue lines, in the first three columns, represent Botucatu city and the MASP region. The gray diamond shape space indicates missing data.

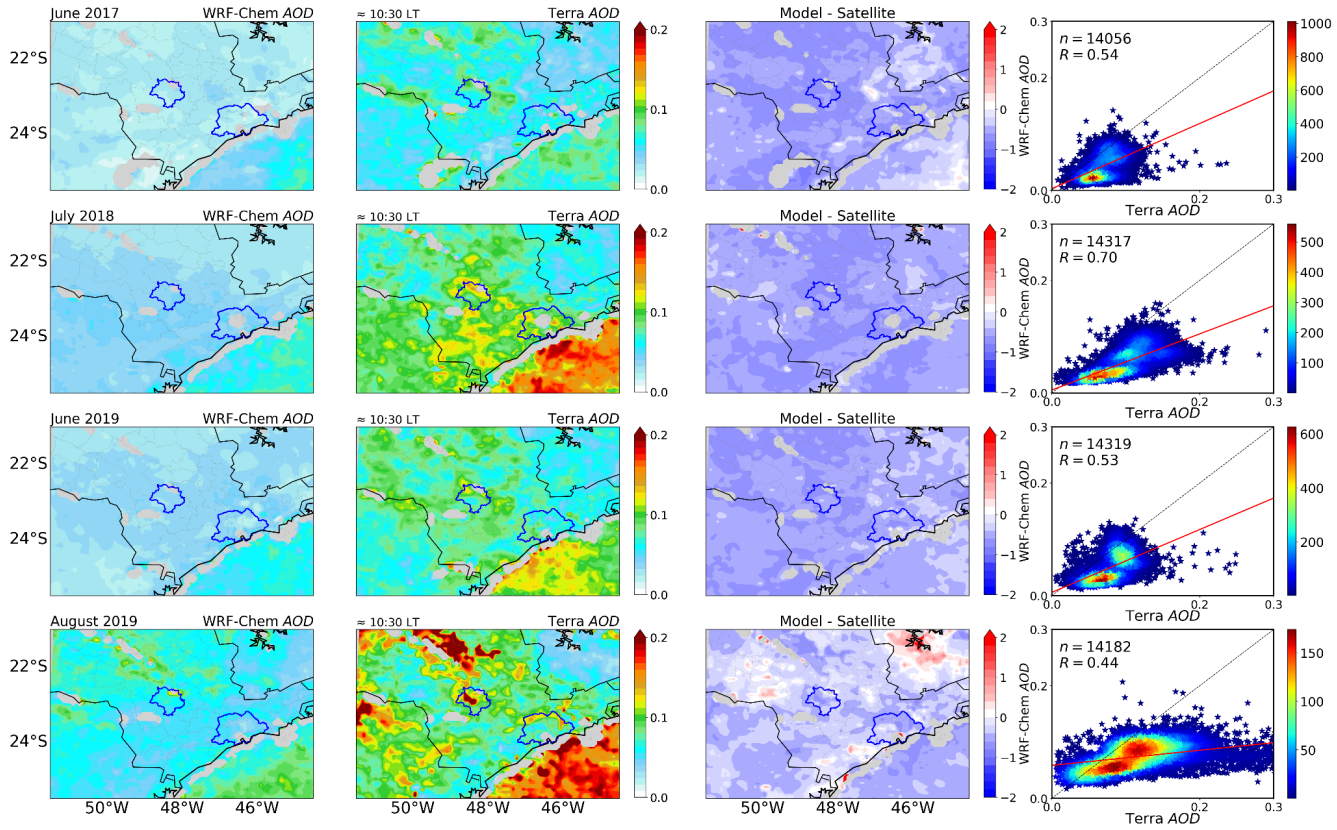

Figure 11: Simulated (first column) and observed (second column) mean spatial distribution of AOD values around at 10:30 LT, over southeastern Brazil for June 2017, July 2018 and June and August 2019. The third and fourth columns represent the relative difference and correlation between both tools. The blue lines, in the first three columns, represent Botucatu city and the MASP and the gray space indicates missing data.

Tables

Table 1: Selected WRF-Chem model configuration options.

Atmospheric Process	WRF-Chem option
Cloud microphysics	Morrison 2-Moment
Boundary Layer	Yonsei University
Cumulus clouds	Grell 3D Ensemble
Longwave radiation	RRTMG
Shortwave radiation	RRTMG
Land surface	Unified Noah Land Surface Model
Surface layer	Revised MM5
Gas-phase chemistry	MOZART
Aerosol chemistry	GOCART
Photolysis	Madronich F-TUV photolysis
Emissions	**Model**
Anthropogenic	LAPAt pre-processors (Andrade et al., 2015)
Biogenic	MEGAN
Fire	FINN
Sea Salt	GOCART sea salt emissions
Aerosol Optical Properties	Based upon volume approximation

Table 2: Additional stations on our study domain.

Stations	**Geo location**	**Latitude (◦)**	**Longitude (◦)**	**Period**	**Parameter**
IAG-USP	Urban Park	-23.65	-46.62	June 2017, July 2018, June and August 2019	T_{2m}, RH_{2m}, WS_{10m} and Precipitation
Botucatu	Regional Urban	-22.85	-48.43	June and August 2019	Meteorological: T_{2m}, WS_{10m}, WD_{10m} and Precipitation. Pollutants: NOx, O_3,CO and $PM_{2.5}$.
* São Paulo	Urban Park	-23.56	-46.74	2014-2019	AOD values
* SP-EACH	Urban Park	-23.48	-46.50	2016-2019	AOD values
∗ Cachoeira Paulista	Regional Urban	-22.68	-45.00	2016-2019	AOD values
∗ Itajuba	Regional Urban	-22.41	-45.45	2014-2019	AOD values

∗ are AERONET stations and their data are freely available on the AERONET website (https://aeronet.gsfc.nasa.gov/)

Table 3: Satellite Configurations.

Characteristics \ Satellite	**Terra**		**Aqua**	**Aura**	**GPM**
Sensor	MODIS	MOPITT	MODIS	OMI	IMERG
Product	MODxx	MOP03T	MYDxx	DOMINIO v2.0	GPM_3IM ERGDF
Level	Level 2	Level 3	Level 2	Level 2	Level 3
Local equator crossing time	10:30	10:30/22:30	13:30	13:45(± 15 minutes)	-
Spatial Resolution	1, 3 and 10 km	1 degree	1, 3 and 10 km	13x24 km^2	10x10 km^2
Temporal Resolution	1 day	1 or 2 per day	1 day	1 day	1 day
Repeat Cycle	16 days	16 days	16 days	16 days	-
Pollutants	AOD[a]	CO[b]	AOD[a]	NO_2[c]	Precipitation[d]

[a]https://ladsweb.modaps.eosdis.nasa.gov/search/
[b]https://asdc.larc.nasa.gov/data/MOPITT/MOP03T.009
[c]www.temis.nl
[d]https://disc.gsfc.nasa.gov/datasets/GPM 3IMERGDF 06/summary

Table 4: Performance statistics of the validation between predicted pollutants and measurements by the AQS.

Type of Region	Chemical species	June - 2017								July - 2018							
		n	R	MB	NMB	ME	NME	RMSE	IOA	n	R	MB	NMB	ME	NME	RMSE	IOA
Regional Urban	NO_x(1h)	697	0.69	-5.33	-26.63	8.47	42.32	11.70	0.76	721	0.78	-12.35	-51.74	13.06	54.74	18.18	0.62
	O_3(1h)	669	0.84	21.01	74.30	21.08	74.56	24.34	0.75	721	0.89	27.35	68.31	27.41	68.46	30.07	0.75
	CO (1h)	685	0.57	-0.45	-69.15	0.45	69.15	0.51	0.45	721	0.62	-0.32	-61.95	0.32	62.12	0.41	0.51
	$PM_{2.5}$(1h)	697	0.43	-9.68	-64.29	9.75	64.72	11.16	0.45	721	0.23	-16.04	-63.01	16.83	66.10	19.52	0.45
	$PM_{2.5}$(24h)	30	0.43	-9.90	-64.38	9.90	64.38	10.44	0.37	31	0.11	-15.41	-60.79	15.68	61.85	16.86	0.33
Urban Park	NO_x(1h)	668	0.40	19.92	52.77	36.65	97.09	52.84	0.58	719	0.42	-0.41	-0.84	33.69	69.19	48.13	0.65
	O_3(1h)	696	0.69	10.52	54.28	17.93	92.48	25.56	0.75	721	0.82	11.45	37.51	18.76	61.45	24.96	0.87
	CO (1h)	564	0.32	0.28	-45.87	0.36	51.63	0.53	0.49	506	0.45	0.07	14.54	0.32	69.07	0.46	0.66
	$PM_{2.5}$(1h)	697	0.52	-4.88	-29.18	8.71	52.09	11.67	0.66	721	0.30	-7.65	-25.58	20.79	69.51	33.52	0.47
	$PM_{2.5}$(24h)	30	0.71	-5.36	-30.40	6.30	35.77	8.66	0.66	31	0.52	-7.82	-26.26	12.74	42.78	15.65	0.68
Urban	NO_x(1h)	697	0.48	-3.76	-6.26	34.02	56.59	45.38	0.70	721	0.58	-27.89	-39.16	37.88	53.19	55.44	0.64
	O_3(1h)	697	0.72	10.74	49.25	16.16	74.11	22.95	0.77	721	0.85	16.61	53.08	19.51	62.34	24.0	0.86
	CO (1h)	697	0.60	-0.36	108.48	0.40	138.86	0.51	0.64	721	0.64	-0.56	-57.71	0.57	58.73	0.77	0.58
	$PM_{2.5}$(1h)	697	0.50	-9.52	-48.66	10.95	56.01	13.98	0.55	721	0.36	-13.37	-38.97	22.59	65.87	32.91	0.56
	$PM_{2.5}$(24h)	30	0.70	-10.24	-49.74	10.24	52.18	12.88	0.52	31	0.58	-13.13	-38.76	14.97	44.20	18.25	0.66
Industrial	NO_x(1h)	668	0.57	0.17	0.68	14.73	58.08	21.06	0.74	188	0.65	-16.77	-46.86	19.61	54.81	30.43	0.62
	O_3(1h)	565	0.79	22.61	146.53	23.70	153.58	30.60	0.72	689	0.84	28.64	84.22	31.04	91.28	36.22	0.80
June - 2019										**August - 2019**							
Regional Urban	NO_x(1h)	649	0.72	-9.24	-44.41	9.91	47.63	14.64	0.63	718	0.81	-5.68	-36.50	6.82	43.82	10.69	0.74
	O_3(1h)	649	0.90	26.83	81.50	26.83	81.52	28.82	0.73	718	0.88	16.63	37.83	17.03	38.74	20.52	0.84
	CO (1h)	649	0.61	-0.27	-59.81	0.27	59.92	0.35	0.49	708	0.73	-0.26	-61.11	0.26	61.27	0.33	0.49
	$PM_{2.5}$(1h)	649	0.48	-11.31	-64.26	11.34	64.47	13.18	0.49	718	0.24	-9.65	-57.89	10.07	60.42	12.65	0.46
	$PM_{2.5}$(24h)	29	0.45	-12.03	-65.26	12.03	65.26	13.14	0.38	30	0.06	-9.67	-57.98	9.79	58.70	11.36	0.43
Urban Park	NO_x(1h)	609	0.27	8.01	23.92	30.20	90.13	45.98	0.51	665	0.42	7.19	25.23	25.25	88.62	44.48	0.61
	O_3(1h)	649	0.84	10.22	37.61	16.98	62.51	22.32	0.86	718	0.79	4.03	10.32	16.04	41.09	21.05	0.87
	CO (1h)	612	0.36	-0.10	-19.63	0.27	54.06	0.46	0.55	484	0.50	-0.13	-25.93	0.27	54.99	0.53	0.59
	$PM_{2.5}$(1h)	648	0.28	-4.89	-27.70	10.39	58.89	16.62	0.49	718	0.35	-3.98	-27.41	8.95	61.69	12.19	0.52
	$PM_{2.5}$(24h)	29	0.46	-5.90	-31.55	8.18	43.73	10.20	0.63	30	0.63	-4.06	-27.83	5.84	40.03	7.56	0.63
Urban	NO_x(1h)	649	0.48	-27.45	-41.94	36.98	55.98	53.51	0.57	718	0.65	-13.22	-27.49	26.12	54.31	38.87	0.76
	O_3(1h)	649	0.86	16.79	66.67	19.24	76.38	23.60	0.82	718	0.80	10.70	30.25	16.59	46.89	21.46	0.84
	CO (1h)	649	0.60	-0.53	-61.34	0.54	61.84	0.71	0.53	718	0.76	-0.34	-54.18	0.35	55.74	0.51	0.61
	$PM_{2.5}$(1h)	649	0.39	-12.84	-55.57	14.25	61.65	19.39	0.53	718	0.49	-7.88	-45.34	10.51	60.54	14.49	0.53
	$PM_{2.5}$(24h)	29	0.39	-15.17	-59.60	15.17	59.60	19.36	0.48	30	0.61	-7.93	-45.52	9.02	51.76	11.17	0.58
Industrial	NO_x(1h)	588	0.61	-8.72	-33.46	13.32	51.12	23.39	0.64	655	0.67	-3.06	-15.24	10.36	51.58	17.23	0.77
	O_3(1h)	561	0.81	31.82	138.68	31.95	139.25	37.90	0.72	686	0.81	30.98	122.17	31.41	123.87	37.10	0.71

The units are O_3 and $PM_{2.5}$ in [μgm^{-3}], NO_x in [ppb] and CO in [ppmv].

Table 5: Performance statistics of the predicted values at the Botucatu station with the measured results.

Variable	June 2019								August 2019							
Meteorological	**n**	**R**	**MB**	**NMB**	**ME**	**NME**	**RMSE**	**IOA**	**n**	**R**	**MB**	**NMB**	**ME**	**NME**	**RMSE**	**IOA**
T_{2m}	505	0.88	-1.17	-5.85	1.64	8.16	2.11	0.90	599	0.88	0.47	2.60	1.98	10.91	2.57	0.94
WS_{10m}	505	0.61	-1.57	-51.22	1.59	51.73	1.72	0.46	599	0.76	-1.84	-45.76	1.86	46.17	2.04	0.57
WD_{10m}	505	-	6.17	3.86	47.87	30.21	-	-	599	-	6.41	4.09	41.54	26.51	-	-
Pollutants	**n**	**R**	**MB**	**NMB**	**ME**	**NME**	**RMSE**	**IOA**	**n**	**R**	**MB**	**NMB**	**ME**	**NME**	**RMSE**	**IOA**
NO_x	308	0.60	0.59	8.02	2.26	49.64	3.13	0.76	579	0.66	1.40	45.33	2.34	75.82	3.36	0.75
O_3	501	0.74	7.46	10.76	12.01	17.33	15.29	0.82	588	0.68	-0.57	-0.85	11.31	16.78	15.32	0.82
CO	412	0.16	-0.45	-75.85	0.45	75.85	0.48	0.35	600	0.45	-0.55	-82.07	0.55	82.07	0.57	0.34
$PM_{2.5}$	496	-0.10	-2.39	-29.77	3.74	46.61	5.18	0.24	412	0.40	-0.47	-6.84	2.77	40.06	3.48	0.65

The units are T_{2m} in [$^{\circ}C$], WS_{10} in [ms^{-1}] and WD_{10} in [degree]. For O_3 and $PM_{2.5}$ in [μgm^{-3}], NO_x in [ppb] and CO in [ppmv]

Table 6: Performance statistics of the validation between model-simulated and satellite-retrieved data for the four periods.

Variable	Periods	n	R	MB	NMB	ME	NME	RMSE	IOA
	June 2017	14751	0.71	-1.07	-66.57	1.09	68.08	1.21	0.59
NO_2	July 2018	14751	0.77	-0.80	-53.46	0.86	57.21	0.96	0.71
	June 2019	14751	0.64	-0.95	-64.32	0.97	65.85	1.14	0.57
	August 2019	14751	0.64	-1.07	-68.09	1.08	68.92	1.20	0.53

Variable	Periods	Daytime								Nighttime							
		n	**R**	**MB**	**NMB**	**ME**	**NME**	**RMSE**	**IOA**	**n**	**R**	**MB**	**NMB**	**ME**	**NME**	**RMSE**	**IOA**
	June 2017	125	0.60	0.18	14.05	0.18	14.05	0.19	0.38	126	0.59	0.11	8.30	0.12	8.68	0.13	0.58
CO	July 2018	126	0.70	0.11	8.17	0.11	8.17	0.13	0.57	126	0.87	0.11	7.55	0.11	7.55	0.11	0.67
	June 2019	126	0.82	0.13	9.69	0.13	9.69	0.13	0.55	126	0.77	0.10	7.36	0.10	7.40	0.11	0.65

Variable	Periods	Terra								Aqua							
		n	**R**	**MB**	**NMB**	**ME**	**NME**	**RMSE**	**IOA**	**n**	**R**	**MB**	**NMB**	**ME**	**NME**	**RMSE**	**IOA**
	June 2017	14056	0.54	-0.03	-37.91	0.03	39.92	0.03	0.56	14161	0.76	-0.01	-15.64	0.01	25.87	0.02	0.84
AOD	July 2018	14317	0.70	-0.04	-44.66	0.04	45.0	0.05	0.60	14240	0.75	-0.03	-35.34	0.03	37.54	0.04	0.71
	June 2019	14319	0.53	-0.03	-36.94	0.03	39.69	0.04	0.57	13849	0.69	-0.01	-15.38	0.02	27.82	0.02	0.80
	August 2019	14182	0.44	-0.04	37.09	0.05	40.06	0.08	0.47	14056	0.65	-0.03	-29.89	0.04	36.08	0.06	0.60

References

Albuquerque, T. T. A, M. F. Andrade, R. Y. Ynoue, D. M. Moreira, W. L. Andreao, F. S. Dos Santos, E. G. S. Nascimento (2018). “WRF-SMOKE-CMAQ modeling system for air quality evaluation in São Paulo megacity with a 2008 experimental campaign data”. In: Environmental Science and Pollution Research 25, pp. 36555–36569. doi: 10.1007/s11356-018-3583-9.

Andrade, M. F., A. Fornaro, R. M. Miranda, A. Kerr, B. Oyama, P. A. Andre, P. Saldiva (2012). “Vehicle emissions and $PM_{2.5}$ mass concentrations in six Brazilian cities”. In: Air Quality, Atmosphere & Health 5, pp. 79–88. doi: 10.1007/s11869-010-0104-5.

Andrade, M. F., R. Y. Ynoue, E. D. Freitas, E. Todesco, A. L. Vara-Vela, S. Ibarra, L. D. Martins, J. A. Martins, V. S. B. Carvalho (2015). “Air quality forecasting system for Southeastern Brazil”. In: Frontiers in Environmental Science 3, pp. 1–14. doi: 10.3389/fenvs.2015.00009.

Andrade, M. F. et al. (2017). “Air quality in the megacity of S˜ao Paulo: Evolution over the last 30 years and future perspectives”. In: Atmospheric Environment 159, pp. 66–82. doi: 10.1016/j.atmosenv.2017.03.051.

Andreão, W. L., M. F. Alonso, P. Kumar, Pinto J. A., Pedruzzi R., Albuquerque T. T. A. (2020). “Top-down vehicle emission inventory for spatial distribution and dispersion modeling of particulate matter”. In: Environmental Science and Pollution Research 27, pp. 35952–35970. doi: 10.1007/s11356-020-08476-y.

Banta, R. M., C. J. Seniff, J. Nielsen-Gammon, L. S. Darby, T. B. Ryerson, R. J. Alvarez, S. P. Sandberg, E. J. Williams, M. Trainer (2005). “A bad air day in Houston”. In: Bulletin of the American Meteorological Society 86, pp. 657–669. doi: 10.1175/BAMS-86-5-657.

Benavente, R. Noelia (2014). “Estudio de la dinámica del espesor óptico de los aerosoles producido por las fuentes naturales y antropogénicas a partir de las imágenes del sensor modis a bordo del satélite Terra y Aqua sobre América del Sur (2000-20012)”.
https://cybertesis.unmsm.edu.pe/bitstream/handle/20.500.12672/4077/Rojas_bn.pdf?sequence=1&isAllowed=y Accessed: 14 September 2022. Bachelor 's dissertation.

— (2022), “Code and Data to assess Air Quality over southeastern Brazil Part I”, Mendeley Data, V2, doi: 10.17632/d2dmnjn7xf.2

— (2022). “Analysis of the Spatial and Temporal Variability of Gases and Particulate Material Concentrations in the São Paulo Metropolitan Region and its Transport to other regions using Satellite Images and Numerical Modeling”. PhD dissertation.

Boersma, K. F. et al. (2011). “An improved tropospheric N O2 column retrieval algorithm for the Ozone Monitoring Instrument”. In: Atmospheric Measurement Techniques 4.9, pp. 1905–1928.

Brito J., Wurm F., Yáñez-Serrano A. M., de Assunção J. V., Godoy J. M., Artaxo P. (2015). “Vehicular Emission Ratios of VOCs in a Megacity Impacted by Extensive Ethanol Use: Results of Ambient Measurements in São Paulo, Brazil”. Environmental Science Technology, vol. 49, p. 11381.

Brito J., Carbone S., A. Monteiro dos Santos D., Dominutti P., de Oliveira Alves N., V. Rizzo L., Artaxo P. (2018). “Disentangling vehicular emission impact on urban air pollution using ethanol as a tracer”. Scientific Reports, vol. 8, p. 1.

Carvalho, Leila, Charles Jones, Ana Silva, Brant Liebmann, Pedro Silva Dias (June 2011). “The South American Monsoon System and the 1970s climate transition”. In: International Journal of Climatology 31, pp. 1248–1256. doi: 10.1002/joc.2147.

CETESB (2017). Companhia de Tecnologia de Saneamento Ambiental: Relatório Anual de Qualidade do Ar no Estado de São Paulo 2015, São Paulo, Brazil. Technical report.

CETESB (2017). Companhia de Tecnologia de Saneamento Ambiental: Relatório Anual de Qualidade do Ar no Estado de São Paulo 2017, São Paulo, Brazil. Technical report.

— (2019). Companhia de Tecnologia de Saneamento Ambiental: Relatório Anual de Qualidade do Ar no Estado de São Paulo 2019, São Paulo, Brazil. Technical report.

— (2021). Companhia de Tecnologia de Saneamento Ambiental: Relatório Anual de Qualidade do Ar no Estado de São Paulo 2021, São Paulo, Brazil. Technical report.

Chang, J. S. et al. (1990). “The regional acid deposition model and engineering model”. In: Acid Deposition: State of Science and Technology.

Changhan, Bae, Cheol Kim Hyun, Kim Byeong-Uk, Kim Soontae (2020). “Surface ozone response to satellite-constrained NO_x emission adjustments and its implications”. In: Environmental Pollution 258, p. 113469. doi: 10.1016/j.envpol.2019.113469.

Chin, M. et al. (2002). “Tropospheric aerosol optical thickness from the GOCART model and comparisons with satellite and sun photometer measurements”. In: Journal of the Atmospheric Sciences 59, pp. 461– 483. doi: 10.1175/1520-0469(2002)059<0461:TAOTFT>2.0.CO;2.

Chudnovsky, A., A. Lyapustin, C. Wang, Y. and Tang, J. Schwartz, P. Koutrakis (2014). “High Resolution Aerosol Data from MODIS Satellite for Urban Air Quality Studies”. In: Central European Journal of Geosciences 6. http://www.degruyter.com/view/j/geo.2014.6.issue- 1/s13533- 012- 0145-4/s13533-012-0145-4.xml Accessed: 08 September 2021, pp. 17–26.

Damascena, A. S., M. A. Yamasoe, V. S. Martins, J. R. Santana, N. R. Benavente, M. P. Sanchez, N. I. Tanaka, S. P. H Nascimento (2021). “Exploring the relationship between high-resolution aerosol optical depth values and ground-level fine particulate matter concentrations in the metropolitan area of São Paulo”. In: Atmospheric Environment 244, pp. 1–10. doi: 10.1016/j.atmosenv.2020.117949.

Darby, L. S. (2005). “Cluster analysis of surface winds in Houston, Texas, and the impact of wind patterns on ozone”. In: Journal of Applied Meteorology and Climatology 44, pp. 1788–1806. doi: 10 . 1175/JAM2320.1.

Deeter, M. N. et al. (2003). “Operational carbon monoxide retrieval algorithm and selected results for the MOPITT instrument”. In: Journal of Geophysical Research: Atmospheres 108.D14.

Dominutti P., Nogueira T., Fornaro A., Borbon A. (2020). “One decade of VOCs measurements in São Paulo megacity: Composition, variability, and emission evaluation in a biofuel usage context”. Science of The Total Environment, vol. 738, p. 139790.

Emery, C., Z. Liu, A. G. Russell, M. T. Odman, G. Yarwood, N. Kumar (2017). “Recommendations on statistics and benchmarks to assess photochemical model performance”. In: Journal of the Air and Waste Management Association 67, pp. 582–598. doi: 10.1080/10962247.2016.1265027.

Emmons, L. K. et al. (2010). “Description and evaluation of the Model for Ozone and Related Chemical Tracers, version 4 (MOZART-4)”. In: Geoscientific Model Development 3, pp. 43–67. doi: 10.5194/gmd-3-43-2010.

Finlayson-Pitts B., Pitts J (2000). “Chemistry of Upper and Lower Atmosphere”.

Freitas, S. R., G. A. Grell, H. Li (2021). “The Grell–Freitas (GF) convection parameterization: recent developments, extensions, and applications”. In: Geoscientific Model Development 14.9, pp. 5393–5411 doi: 10.5194/gmd-14-5393-2021.

Freitas, S. R. et al. (2007). “Including the sub-grid scale plume rise of vegetation fires in low resolution atmospheric transport models”. In: Atmospheric Chemistry and Physics 7, pp. 3385–3398. doi: 10.5194/ACP-7-3385-2007.

Gavidia-Calderón, M. E. (Nov. 2020). “From Global to local: A multi-scale air quality modeling study over the Metropolitan Area of São Paulo [tese]. São Paulo”. Access 2022-01-26. PhD dissertation. Instituto de Astronomia, Geofísica e Ciências Atmosféricas. doi: 10.11606/T.14.2020.tde-15042021-115527.

Gavidia-Calderón, M. E., A. L. Vara-Vela, N. M. Crespo, M. F. Andrade (2018). “Impact of time-dependent chemical boundary conditions on tropospheric ozone simulation with WRF-Chem: An experiment over the Metropolitan Area of S˜ao Paulo”. In: Atmospheric Environment 195, pp. 112–124. doi: 10.1016/j.atmosenv.2018.09.026.

Grell, G. A., S. R. Freitas, M Stuefer, Fast J. (2011). “Inclusion of biomass burning in WRF-Chem:
impact of wildfires on weather forecasts”. In: Atmospheric Chemistry and Physics 11, pp. 5289–5303. doi: 10.5194/acp-11-5289-2011.28

Grell, G. A., S. E. Peckham, R. Schmitz, S. A. McKeen, G. Frost, W. C. Skamarock, B. Eder (2005). “Fully coupled “on-line” chemistry within the WRF model”. In: Atmospheric Environment 39, pp. 6957–6976. doi: 10.1016/j.atmosenv.2005.04.027.

Guenther, A., T. Karl, P. Harley, C. Wiedinmyer, P. I. Palmer, C. Geron (2006). “Estimates of global terrestrial isoprene emissions using MEGAN (Model of Emissions of Gases and Aerosols from Nature)”. In: Atmospheric Chemistry and Physics 6, pp. 3181–3210. doi: 10.5194/acp-6-3181-2006.

Hertel O., Salmond J., Bloss W. (2009). “Air quality in urban environments”. vol. 28, Royal Society of Chemistry.

Hoelzemann, J. J., K. M. Longo, R. M. Fonseca, N. M. E. do Ros´ario, H. Elbern, S. R. Freitas, C. Pires (2009). “Regional representativity of AERONET observation sites during the biomass burning season in South America determined by correlation studies with MODIS Aerosol Optical Depth”. In: Journal of Geophysical Research: Atmospheres 114, pp. D13301, 1–20. doi: 10.1029/2008JD010369.

Holben, B. et al. (2001). “An emerging ground-based aerosol climatology: Aerosol Optical Depth from AERONET”. In: Journal of Geophysical Research 106, pp. 12, 067–12, 097. doi: 10.1029/2001JD900014.

Hsu, A., A. Reuben, D. Shindell, A. de Sherbinin, M. Levy (2013). “Toward the next generation of air quality monitoring indicators”. In: Atmospheric Environment 80, pp. 561–570. doi: 10.1016/j.atmosenv.2013.07.036.

Hsu, N., S. Tsay, M. King, J. Herman (2004). “Aerosol properties over bright-reflecting source regions”. In: IEEE Transactions on Geoscience and Remote Sensing 42, pp. 557–569. doi: 10.1109/TGRS.2004. 824067.

Huffman, G. J., D. T. Bolvin, D. Braithwaite, K. Hsu, R. Joyce, C. Kidd, E. J. Nelkin, P. Xie (2015). “NASA Global Precipitation Measurement Integrated Multi-Satellite Retrievals for GPM (IMERG)”. In: Algorithm Theoretical Basis Document, version 4.5. http://pmm.nasa.gov/sites/default/files/document_files/IMERG_ATBD_V4.5.pdf. Accessed: 17 March 2022, p. 30.

IBGE (2020). “Estimativa de população. 1 base de dados eletrônicos (portal). Tema: Estatísticas”. In: https://www.ibge.gov.br/estatisticas-novoportal/sociais/populacao/9103-estimativas-de-populacao.html?&t=downloads Accessed: February 2021.

Ichoku, C., D.A. Chu, S. Mattoo, Y.J. Kaufman, L.A. Remer, D. Tanre, I. Slutsker, B.N Holben (2002). “A spatio-temporal approach for global validation and analysis of MODIS aerosol products”. In: Geophysical Research Letters 29, MOD1–4. doi: 10.1029/2001GL013206.

Joyce, R. J., J. E. Janowiak, P. A. Arkin, P. Xie (2004). “CMORPH:A method that produces global precipitation estimates from passive microwave and infrared data at high spatial and temporal resolution”. In: Journal of Hydrometeorology - American Meteorological Society 5, pp. 487–503. doi: 10.1175/1525-7541(2004)005,0487:CAMTPG.2.0.CO;2.

Kanakidou, Maria et al. (2005). “Organic aerosol and global climate modelling: a review”. In: Atmospheric Chemistry and Physics 5.4, pp. 1053–1123.

Kaufman, Y. J., O. Boucher, D. Tanre, M. Chin, L. A. Remer, T. Takemura (2005a). “Aerosol anthropogenic component estimated from satellite data”. In: Geophysical Research Letters 32, pp. L17804, 1– 4. doi: 10.1029/2005GL023125.

Kaufman, Y. J., I. Koren, L. A. Remer, D. Tanre, P. Ginoux, S. Fan (2005b). “Dust transport and deposition observed from the Terra-Moderate Resolution Imaging Spectroradiometer (MODIS) spacecraft over the Atlantic Ocean”. In: Journal of Geophysical Research 110, D10S12, 1–16. doi: 10.1029/2003JD004436.

Kaufman, Y. J., D. Tanré, L. A. Remer, E. Vermote, A. Chu, B. N.Holben (1997). “Operational remote sensing of tropospheric aerosol over land from EOS Moderate Resolution Imaging Spectroradiometer”. In: Journal of Geophysical Research 102, pp. 17, 051–067. doi: 10.1029/96JD03988.

Kota, S. H., H. Zhang, G. Chen, G. W. Schade, Q. Ying (2014). “Evaluation of on-road vehicle CO and NO_x National Emission Inventories using an urban-scale source-oriented air quality model”. In: Atmospheric Environment 85, pp. 99–108. issn: 1352-2310. doi: 10.1016/j.atmosenv.2013.11.020.

Kumar, Rajesh, Manish Naja, G. Pfister, M. Barth, Christine Wiedinmyer, Guy Brasseur (May 2012).“Simulations over South Asia using the Weather Research and Forecasting model with Chemistry (WRF-Chem): Chemistry evaluation and initial results”. In: Geoscientific Model Development 5, pp. 619–648. doi: 10.5194/gmd-5-619-2012.

Lacasaña, M., A. Clemente, I. Romieu (1999). “Evolución de la contaminación del aire e impacto de los programas de control en tres megaciudades de América Latina”. In: Salud Pública de México [en linea] 41. https://www.redalyc.org/articulo.oa?id=10641308 Accessed: 26 January 2022, pp. 203–215.

Lamarque, J. F. et al. (2012). “CAM-chem: description and evaluation of interactive atmospheric chemistry in the Community Earth System Model”. In: Geoscientific Model Development 5, pp. 369–411. doi: 10.5194/gmd-5-369-2012.

Lyapustin, A., Y. Wang, S. Korkin, D. Huang (2018). “MODIS Collection 6 MAIAC algorithm”. In: Atmospheric Measurement Techniques 11, pp. 5741–5765. doi: 10.5194/amt-11-5741-2018.

Mar, K. A., N. Ojha, A. Pozzer, T. M. Butler (2016). “Ozone air quality simulations with WRF-Chem (v3.5.1) over Europe: model evaluation and chemical mechanism comparison”. In: Geoscientific Model Development 9, pp. 3699–3728. doi: 10.5194/gmd-9-3699-2016.

Martins, L. D. et al. (2006). “Emission factors for gas-powered vehicles traveling through road tunnels in São Paulo, Brazil”. In: Environmental science & technology 40, pp. 6722–6729. doi: 10.1021/es052441u.

Martins, L. D. et al. (2018). “Long-range Transport of Aerosols from Biomass Burning over Southeastern South America and their Implications on Air Quality”. In: Aerosol and Air Quality Research 18, pp. 1734–1745. doi: 10.4209/aaqr.2017.11.0545.

Martins, V. S., A. Lyapustin, L. A. S. de Carvalho, C. C. F. Barbosa, E. M. L. M. Novo (2017). “Validation of high-resolution MAIAC aerosol products over South America ". In: Journal of Geophysical Research Atmosphere 122, pp. 7537–7559. doi: 10.1002/2016JD026301.

Miranda R. M., de Fatima Andrade M., Dutra Ribeiro F. N., Mendon ̧ca Francisco K. J., Pérez-Martínez P. J. (2018). “Source apportionment of fine particulate matter by positive matrix factorization in the metropolitan area of São Paulo, Brazil”. Journal of Cleaner Production, vol. 202, p. 253–263.

Molders, N., Kramm G. (2010). “A case study on wintertime inversions in Interior Alaska with WRF”. In: Atmospheric Research 95, pp. 314–332. doi: 10.1016/j.atmosres.2009.06.002.

Monk, K. et al. (2019). “Evaluation of Regional Air Quality Models over Sydney and Australia: Part 1—Meteorological Model Comparison”. In: 10.7. doi: 10.3390/atmos10070374.

Nascimento, Janaina P. et al. (2020). “Aerosols from anthropogenic and biogenic sources and their interactions: modeling aerosol formation, optical properties and impacts over the central Amazon Basin”. In: Atmospheric Chemistry and Physics 21, pp. 6755–6779. doi: 10.5194/acp-2020-1002.

Nascimento, Janaina P. et al. (2022). “Major Regional-Scale Production of O3 and Secondary Organic Aerosol in Remote Amazon Regions from the Dynamics and Photochemistry of Urban and Forest Emissions”. In: Environmental Science & Technology 56.14, pp. 9924–9935. doi: 10.1021/acs.est.2c01358.

Nogueira, T. et al. (2021). “BEvolution of Vehicle Emission Factors in a Megacity Affected by Extensive Biofuel Use: Results of Tunnel Measurements in São Paulo, Brazil”. In: npj Climate and Atmospheric Science 55(10), pp. 6677–6687. doi: 10.1021/acs.est.1c01006.

Pérez-Martínez, P. J., Andrade M. F., R. M. de Miranda (2015). “Traffic-related air quality trends in São Paulo, Brazil”. In: Journal of Geophysical Research: Atmospheres 120, pp. 6290–6304. doi: 10.1002/2014JD022812.

Popescu, F., and Ionel, I. (2010). “Anthropogenic air pollution sources”. Air quality, 1-22.

Remer, L. A. et al. (2005). “The MODIS aerosol algorithm, products, and validation”. In: Journal of the Atmospheric Sciences 62, pp. 947–973. doi: 10.1175/JAS3385.1.

Roy, P. S., M. D. Behera, S. K. Srivastav (2017). “Satellite remote sensing: sensors, applications and techniques”. In: Proceedings of the National Academy of Sciences, India Section A: Physical Sciences 87.4, pp. 465–472. doi: 10.1007/s40010-017-0428-8.

Rozante J. R., Rozante V., Souza Alvim D., Ocimar Manzi A., Barboza Chiquetto J., Siqueira D’Amelio M. T., Moreira D. S. (2017). “Variations of Carbon Monoxide Concentrations in the Megacity of São Paulo from 2000 to 2015 in Different Time Scales”. Atmosphere, vol. 8.

Ruibin, Xue, Wang Shanshan, Zhang Sanbao, He Siyu, Liu Jiaqi, Tanvir Aimon, Zhou Bin (2022). “Estimating city NO_X emissions from TROPOMI high spatial resolution observations – A case study on Yangtze River Delta, China”. In: Urban Climate 43, p. 101150. issn: 2212-0955. doi: https://doi.org/10.1016/j.uclim.2022.101150.

Sarkar, M., Venkataraman C., Guttikunda S., Sadavarte P. (2016). “Indian emissions of technology-linked NMVOCs with chemical speciation: an evaluation of the SAPRC99 mechanism with WRF-CAMx simulations”. In: Atmospheric Environment 134, pp. 70–83. doi: 10.1016/j.atmosenv.2016.03.037.

Schuch, D. A., Ibarra S., Freitas E. D., Andrade M. F. (2018). “emissV: A Preprocessor for WRF-Chem Model”. In: Journal of Atmospheric Science Research 1, p. 1.

Silva, R. S., M. F. Andrade (2013). “Validação de poluentes fotoquímicos e inclusão do inventário de emissões no modelo de qualidade do ar WRF/CHEM, para a região metropolitana de São Paulo”. In: Revista Brasileira de Meteorologia 28, pp. 105–121. doi: 10.1590/S0102-77862013000100010.

Squizzato, R., Nogueira T., Martins L. D., Martins J. A., Astolfo R., Machado C. B., Andrade M. F., Freitas E. D. (2021). “Beyond megacities: tracking air pollution from urban areas and biomass burning in Brazil”. In: npj Climate and Atmospheric Science 4, p. 17. doi: 10.1038/s41612-021-00173-y.

Tang, Wenfu et al. (Mar. 2020). “Assessing Measurements of Pollution in the Troposphere (MOPITT) carbon monoxide retrievals over urban versus non-urban regions”. In: Atmospheric Measurement Techniques 13, pp. 1337–1356. doi: 10.5194/amt-13-1337-2020.

Tie, X., Fuhai Geng, Li Peng, Wei Gao, Chunsheng Zhao (2009). “Measurement and modeling of O_3 variability in Shanghai, China: Application of the WRF-Chem model”. In: Atmospheric Environment 43.28, pp. 4289–4302. doi: 10.1016/j.atmosenv.2009.06.008.

Tie, X., Madronich S., Walters S., Zhang R., Racsh P., Collins W. (2003). “Effect of clouds on photolysis and oxidants in the troposphere”. In: Journal of Geophysical Research 108(D20), p. 4642. doi: 10.1029/2003JD003659.

Tie, X. et al. (2013). “Megacity impacts on regional ozone formation: observations and WRF-Chem modeling for the MIRAGE-Shanghai field campaign”. In: Atmospheric Chemistry and Physics 13, pp. 5655–5669. doi: 10.5194/acp-13-5655-2013.

Valin, L. C., A. R. Russell, R. C. Hudman, R. C. Cohen (2011). “Effects of model resolution on the interpretation of satellite NO_2 observations”. In: Atmospheric Chemistry and Physics 11.22, pp. 11647–11655. doi:10.5194/acp-11-11647-2011.

Vara - Vela, A. L., M. F. Andrade, Kumar P., Ynoue R. Y., Muñoz A. G. (2016). “Impact of vehicular emissions on the formation of fine particles in the Sao Paulo Metropolitan Area: a numerical study with the WRF-Chem model”. In: Atmospheric Chemistry and Physics 16, pp. 777–797. doi: 10.5194/acp-16-777-2016.

Vara - Vela, A. L., M. F. Andrade, Zhang Y., Kumar P., Ynoue R. Y., Souto-Oliveira C. E., Silva L. F., Landulfo E. (2018). “Modeling of atmospheric aerosol properties in the Sao Paulo Metropolitan Area: Impact of biomass burning”. In: Journal of Geophysical Research 123, pp. 9935–9956. doi: 10.1029/2018JD028768.

Vara - Vela, A. L., L. D. Herdies, Alvim D. S., Vendrasco E. P., Figueroa S. N., Pendharkar J., Fernandez J. P. R. (2021). “A New Predictive Framework for Amazon Forest Fire Smoke Dispersion over South America”. In: Bulletin of the American Meteorological Society 102, pp. 1700–1713. doi: 10.1175/BAMS-D-21-0018.1.

WHO (2021). WHO global air quality guidelines: particulate matter ($PM_{2.5}$ and PM_{10}), ozone, nitrogen dioxide, sulfur dioxide and carbon monoxide. World Health Organization, xxi, 273 p.

Wiedinmyer, C., S. K. Akagi, R. J. Yokelson, L. K. Emmons, J. A. Al-Saadi, J. J. Orlando, A. J. Soja (2011). “The Fire Inventory from Ncar (FINN): A High Resolution Global Model to Estimate the Emissions from Open Burning”. In: Geoscientific Model Development 4, pp. 625–641. doi: 10.5194/gmd-4-625-2011.

Zaveri, R. A., Peters L. K. (1999). “A new lumped structure photochemical mechanism for large-scale applications”. In: Journal of Geophysical Research 104, pp. 30387–30415. doi: 10.1029/1999JD900876.